Molecular Therapy
Nucleic Acids
Original Article

Investigating discovery strategies and pharmacological properties of stereodefined phosphorodithioate LNA gapmers

Jörg Duschmalé,[1] Adrian Schäublin,[1] Erik Funder,[2] Steffen Schmidt,[2] Łukasz J. Kiełpiński,[2] Helle Nymark,[2] Klaus Jensen,[2] Troels Koch,[2] Martina Duschmalé,[3] Erich Koller,[3] Marianne Ravn Møller,[3] Simone Schadt,[3] Christophe Husser,[3] Andreas Brink,[3] Sabine Sewing,[3] Tanja Minz,[3] Jesper Wengel,[4] Konrad Bleicher,[1] and Meiling Li[1]

[1]Pharma Research and Early Development, Therapeutic Modalities, Roche Innovation Center Basel, F. Hoffmann-La Roche Ltd., 4070 Basel, Switzerland; [2]Pharma Research and Early Development, Therapeutic Modalities, Roche Innovation Center Copenhagen A/S, Femtidsvej 3, 2970 Hørsholm, Denmark; [3]Pharma Research and Early Development, Pharmaceutical Sciences, Roche Innovation Center Basel, F. Hoffmann-La Roche Ltd., 4070 Basel, Switzerland; [4]Biomolecular Nanoscale Engineering Center, Department of Physics, Chemistry and Pharmacy, University of Southern Denmark, 5230 Odense M, Denmark

The introduction of sulfur into the phosphate linkage of chemically synthesized oligonucleotides creates the stereocenters on phosphorus atoms. Researchers have valued the nature of backbone stereochemistry and early on investigated drug properties for the individual stereocenters in dimers or short oligomers. Only very recently, it has become possible to synthesize fully stereodefined antisense oligonucleotides in good yield and purity. Non-bridging phosphorodithioate (PS_2) introduces second sulfur into the phosphorothioate linkage to remove the chirality of phosphorus atom. Here, we describe the application of symmetrical non-bridging PS_2 linkages in the context of stereodefined locked nucleic acids (LNAs) antisense oligonucleotides with the goal of reducing chiral complexity and, ultimately, resulting in single molecules. In addition, we propose a rather simple strategy to rapidly identify stereodefined gapmers, combining PS_2 and a preferred stereochemistry motif (RSSR), which supports RNase-H-mediated target knockdown. Pharmacological efficacy and metabolic stability are investigated systematically using *ApoB* as a target sequence, where *in vivo* data correlate well to what is observed *in vitro*.

INTRODUCTION

One of the first issues medicinal chemists would address in any given lead optimization program is the understanding of chirality in potential drug candidates that feature unresolved stereocenters. Countless examples have been reported, both for small molecules[1] and oligonucleotides,[2] where the resolution and inversion of chiral centers demonstrated substantial impact on drug properties, such as potency or safety. As the introduction of sulfur into the backbone of oligonucleotides leads to such unresolved stereocenters, academic groups around Stec et al.[3] and Guga and Stec[4] have pioneered the enantioselective synthesis of such internucleoside linkages, setting the stage for investigating the impact of "phosphate chirality." Meanwhile, several approaches are established that do allow the synthesis of fully stereodefined phosphorothioate antisense oligonucleotides in good yield and purity.[5,6] Different groups[7–9] have reported the pharmacological profiles of such stereodefined antisense oligonucleotides with a seminal paper published by Verdine et al.,[10] clearly describing the impact of chirality on various properties for the individual molecules, such as target binding, lipophilicity, or *in vivo* efficacy, and therefore, controlling chirality can potentially enhance overall therapeutic profiles of antisense oligonucleotides.

While modern synthetic schemes now allow for the stereocontrolled synthesis of phosphorothioate (PS) linkages and, therefore, provide access to single isomers, given the high complexity of generally 10^3–10^5 possibilities, it is unlikely to find single diastereoisomers with improved properties compared with the averaged properties of the overall mixture without a suitable strategy. For example, a conventionally synthesized 20-mer antisense oligonucleotide (ASO) with 19 non-stereodefined PS linkages contains a mixture of 2^{19} = 524,288 diastereoisomers. Given the high number of possible diastereoisomers and the difficulty in finding single diastereoisomers with improved properties, a strategy on rapid identification of fully stereodefined PS-ASOs will offer a new dimension to the RNA therapeutic field. One potential approach to reduce this diastereoisomeric complexity is to insert symmetrical ("non-chiral") thiophosphate modifications, since every "non-chiral" linkage introduced into the oligonucleotide reduces the overall number of possible diastereoisomers by 50%.[11]

Here, we report the systematic insertion of non-bridging phosphorodithioate (PS_2) into the flank region of locked nucleic acids (LNAs) gapmers and investigate target engagement, mRNA knockdown,

Received 14 January 2022; accepted 15 June 2022;
https://doi.org/10.1016/j.omtn.2022.06.010.

Correspondence: Meiling Li, Pharma Research and Early Development, Therapeutic Modalities, Roche Innovation Center Basel, F. Hoffmann-La Roche Ltd., 4070 Basel, Switzerland.
E-mail: meiling.li@roche.com

A

ID	Design[c]	IC_{50}[d] (μM)	Tm[a,d] (°C)	Rt[b]
RTR3833	G•C•a•t•t•g•g•t•a•t•T•C•A	0.16±0.02	55.9±0.8	13.2
ASO-1	G°C•a•t•t•g•g•t•a•t•T•C•A	0.11±0.02	57.4±1.5	13.0
ASO-2	G•C•a•t•t•g•g•t•a•t•T•C°A	0.17±0.04	57.1±0.8	13.0
ASO-3	G°C•a•t•t•g•g•t•a•t•T•C°A	0.12±0.03	57.4±0.7	13.1
ASO-4	G°C•a•t•t•g•g•t•a•t•T°C°A	0.15±0.02	56.5±0.9	13.2
ASO-5	G°C°a•t•t•g•g•t•a•t•T•C°A	0.07±0.01	57.5±0.5	13.2
ASO-6	G°C°a•t•t•g•g•t•a•t•T°C°A	0.08±0.01	55.8±0.8	13.2
*All-PS_2	G°C°a°t°t°g°g°t°a°t°T°C°A	nd	53.7±3.2	13.9
*All-PO	G•C•a•t•t•g•g•t•a•t•T•C•A	nd	64.2±1.6	9.7

Figure 1. *In vitro ApoB* mRNA target reduction in primary mouse hepatocytes (PMHs) after 72 h of gapmer ASOs exposure

Reduction of target *ApoB* mRNA was quantified by qRT-PCR. All experiments are carried out in triplicates. (A) Design, antisense activity, Tm (melting temperature), and Rt (retention time) are shown. Positions of phosphorodithioate (PS_2) (yellow °) are shown while the rest of ASO is stereorandom PS modified. ASOs marked with asterisk (*) were tested in a different experiment following the same screening condition. [a]Melting temperature to complementary RNA (Tm) is shown; complementary RNA for Tm measurement is as follows: UGAAUACCAAUGC. [b]RP-HPLC retention time (Rt) is shown. [c]Upper case designates LNA nucleotide and lower case designates DNA nucleotide, with symbols designating stereorandom PS (•), PS_2 (yellow °), and phosphate (red •). [d]Standard deviation (±) is shown; nd, not determined. (B) Dose-response curves for reducing *ApoB* mRNA in PMHs are shown.

B

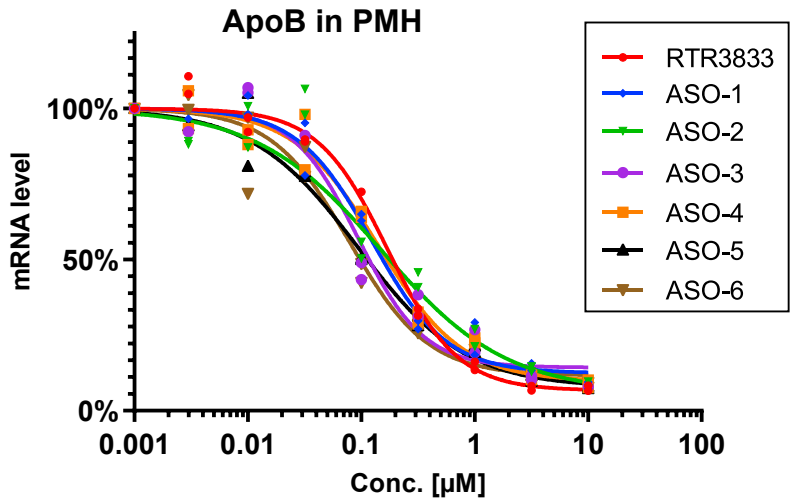

lipophilicity, and *in vitro* toxicity of the resulting PS_2-modified ASOs. Furthermore, we suggest a discovery strategy for the rapid identification of single molecules by combining the PS_2-modified flanks with fully stereodefined PS linkages in the gap region. A substantially increased *in vivo* efficacy was observed for an anti-*ApoB* stereodefined PS_2 LNA gapmer, outperforming both its parent (diastereomeric mixture) as well as a fully stereodefined monothioate analog thereof.

RESULTS

Target engagement, lipophilicity, and mRNA knockdown of phosphorodithioate-modified LNA gapmers

Symmetrical PS_2, where both non-bridging oxygen atoms within the phosphate group are replaced by sulfur, have been introduced by Caruthers[12–20] and also further investigated by other groups.[21–38] Nonetheless, PS_2 modifications remained rather unexplored in ASOs, which might be due to somewhat inconsistent and partly unfavorable data reported previously.[14,16,20,37] We revisited the PS_2 modification and hypothesized that the diligent introduction of only a limited number of PS_2 groups at defined positions within AOSs should be well tolerated and may show improved drug properties when compared with fully PS-modified ASOs. Exemplified for RTR3833, a well-characterized anti-*ApoB* ASO,[39] six PS_2 analogs thereof were generated (ASO-1–ASO-6), where the PS_2 content was increased subsequently in flank regions only. All analogs have been tested for their target knockdown efficacy in mouse primary hepatocytes as represented in Figure 1A. The half-maximal inhibitory concentration (IC_{50}) values were generated by exposing the cells with ASOs for 72 h under gymnotic uptake conditions, i.e., no transfection reagents added (Figure 1B). All compounds performed equally good or better compared with RTR3833. With respect to target engagement (RNA binding), no meaningful change is observed for PS_2-modified ASO-1–ASO-6 (see target engagement [Tm] in Figure 1A). As a measure of lipophilicity, we have investigated the impact of PS_2 to the retention time (Rt) in reversed phase high performance liquid chromatography (HPLC). Under the given analytical conditions, the reference PS ASO (RTR3833) elutes with a retention time of Rt = 13.2 min. No meaningful difference is observed for ASO-1–ASO-6 (Figure 1A). For reference, we also generated and analyzed the all-PS_2 as well as the corresponding phosphate (all-PO) analogs (Figure 1A). While for the full PS_2-modified sequence, only a slightly higher retention time is observed (all-PS_2: Rt = 13.9 min), the Rt for the all-PO analog is substantially lower (all-PO: Rt = 9.7 min) compared with the

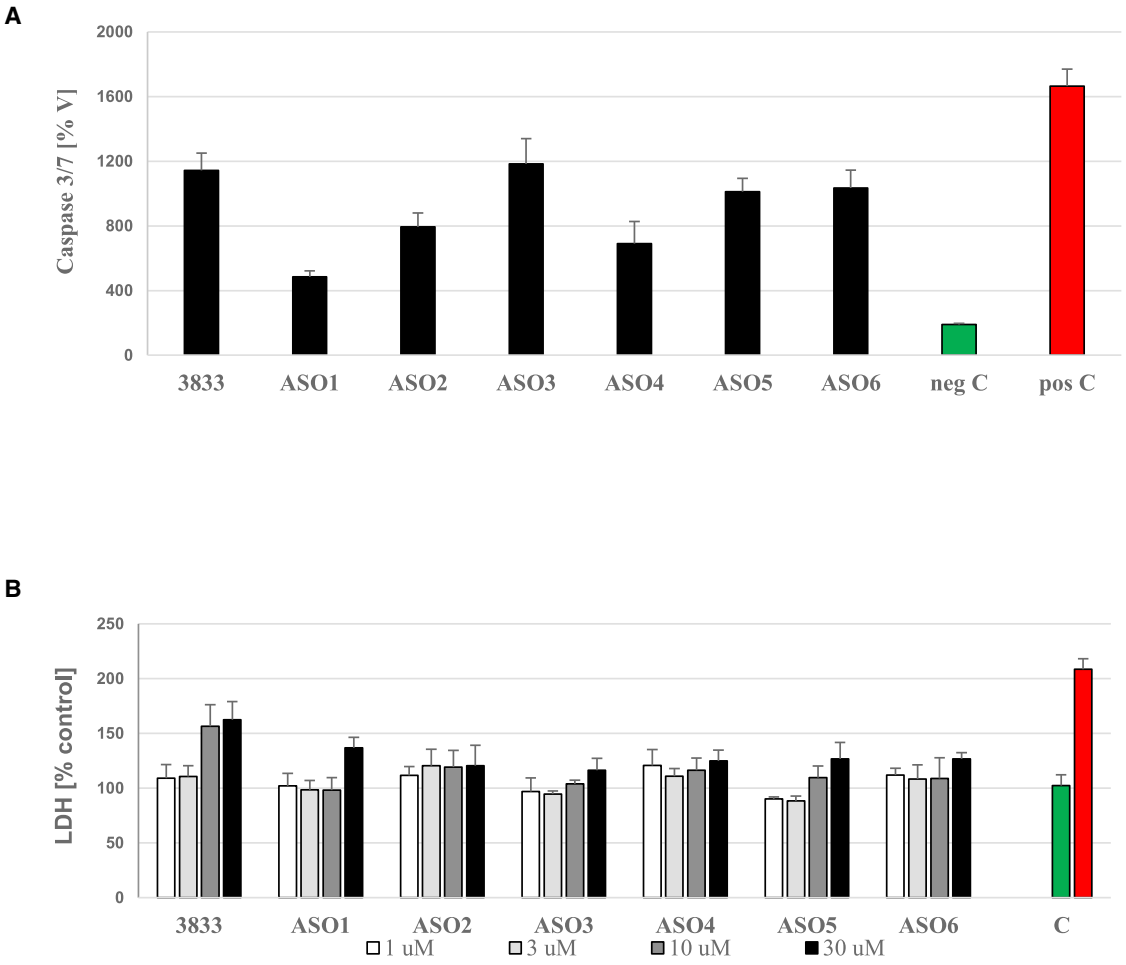

Figure 2. *In vitro* safety profile of phosphorodithioates by caspase 3/7 activation and LDH secretion

(A) *In vitro* safety profile of PS_2 in *HepG*$_2$ cells 24 h after transient transfection at 100 nM concentration determined by caspase 3/7 activation. Bars (%V) represent mean of the relative caspase activity of tested compounds to the vehicle control (culture medium). Negative control in green bar and positive control in red bar are included. (B) *In vitro* safety profile of PS_2 in primary mouse hepatocytes determined by LDH secretion after 3 days of gymnotic uptake with negative (green) and positive (red) controls tested at 30 μM is shown. Bars (% control) represent mean of the relative secreted LDH of tested compounds to the vehicle control (culture medium).

reference ASO (RTR3833). This indicates that the increase of lipophilicity is only marginal when introducing PS_2 linkages sparingly into otherwise PS-modified ASOs.

Further studies were executed for other target sequences, leading to very similar results, i.e., symmetrical, non-bridging PS_2 functionalities introduced in the flank region of LNA gapmers show no significant impact on Tm or *in vitro* potency (Figures S1 and S2 in supplemental material) and may therefore be used to reduce chiral complexity in any given ASO design.

Assessment of potential toxicity *in vitro*

In order to assess whether PS_2 modifications pose an increased toxicity threat, we have evaluated the potential risk of such phosphate bioisosteres *in vitro*. The hepatotoxicity potential was assessed after transient transfection of HepG2 cells by monitoring caspase 3/7 activation as reported earlier (Figure 2A).[40] None of the modifications induced any increase in caspase activation compared with the parent RTR3833. In addition, we investigated the hepatotoxicity potential in primary mouse hepatocytes after gymnotic uptake (Figure 2B). Again, none of the modifications resulted in worsening the mild toxicity seen with RTR3833 as measured by lactate dehydrogenase (LDH) release into the supernatant.

Discovery strategy for the rapid *in vitro* identification of stereodefined phosphorodithioate LNA gapmers

It is well accepted in the ASOs community that primarily the RNA target region, and therefore the drug sequence, as well as the overall ASO architecture (high-affinity entities, i.e., LNA, 2′-O-methoxyethylribose [MOE], etc. versus DNA) are the main drivers for pharmacology.[2,41] Insofar as the pharmacokinetics and pharmacodynamics profile of a given, classically synthesized PS ASO can be further

A

ID	Design[a]	DIs[b]	IC_{50}[c] (μM)
RTR3833	G•C•a•t•t•g•g•t•a•t•T•C•A	4096	0.18±0.01
ASO-7	G•C^a^t^t^g^g•t•a•t•T^C^A	16	0.22±0.01
ASO-8	G•C^a•t^t^g^g^t•a•t•T^C^A	16	0.27±0.04
ASO-9	G•C^a•t•t^g^g^t^a•t•T^C^A	16	0.08±0.01
ASO-10	G•C^a•t•t•g^g^t^a^t•T^C^A	16	0.10±0.04
ASO-11	G•C^a•t•t•g•g^t^a^t^T^C^A	16	0.20±0.03

B

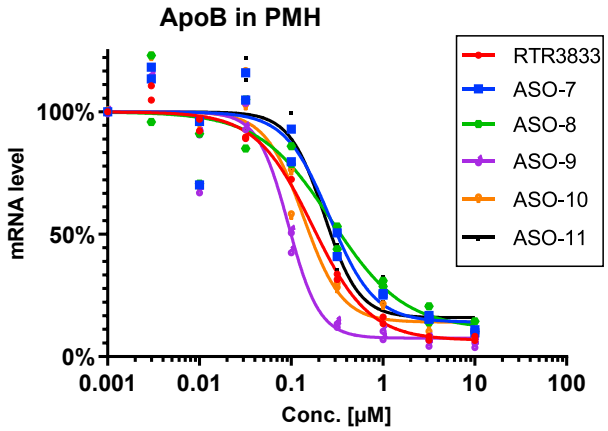

Figure 3. *In vitro ApoB* mRNA target reduction in primary mouse hepatocytes (PMHs) after 72 h of gapmer ASOs exposure

Reduction of target *ApoB* mRNA was quantified by qRT-PCR. All experiments are carried out in triplicate. (A) Design, diastereoisomers (DIs), and antisense activity are shown. Positions of PS_2 (yellow °) and RSSR motif (red ^, green v, green v, red ^) are shown, while the rest of ASO is stereorandom PS modified. [a]Upper case designates LNA nucleotide, lower case designates DNA nucleotide, and symbols designate stereorandom PS (•), PS_2 (yellow °), R configuration (red ^), and S configuration (green v). [b]DIs designates diastereoisomers. [c]Standard deviation (±) is shown. (B) Dose-response curves for reducing *ApoB* mRNA in PMHs are shown.

improved by evolving diastereoisomeric mixtures into partially or fully stereodefined single molecules is currently under debate.[7,8,10] To address this question in the context of LNA gapmers, we investigated and further optimized the anti-*ApoB* lead sequence RTR3833. Since all PS internucleoside linkages were introduced via state-of-the-art phosphoramidite chemistry, this ASO results in an inseparable mixture of potentially 2^{12} = 4,096 diastereoisomers (DIs). It is a high workload to synthesize and test all 4,096 DIs to identify a single DI with improved properties. Therefore, a rapid strategy for single-molecule identification is necessary. Having demonstrated the tolerability of non-bridging PS_2 introduced in the flank region of classical gapmers, we wanted to take advantage of their symmetry and therefore introduced two of these modifications at both ends of LNA sequence of RTR3833, thereby reducing the number of possible DIs from 4,096 to 256 (ASO-6 Figure 3A). Verdine et al.[10] have introduced and rationalized the stereo motif 3′-SSR to support RNase-H-mediated target cleavage in stereodefined ASOs. We have made similar observations for a stereo quadruplet RSSR when positioned appropriately in the gap region of the ASO (Figures S3A and S3B in supplemental material). It was observed that RSSR stereo motif in a specific position in DNA gap can enhance the chance of finding a potent fully stereodefined ASO. Based on this finding, we wanted to further exploit the stereo quadruplet in combination with the achiral PS_2 introduced in the flank regions. All possible analogues were generated, where this stereo motif was moved in a consecutive manner through the DNA gap region while leaving the remaining PS internucleoside linkages racemic (called RSSR walk). Thus, five partially stereodefined PS_2 hybrid ASOs resulted, which now consist of 16 DIs only (Figure 3A). The oligonucleotides were synthesized by means of solid-phase oligonucleotide chemistry similar to those reported in the literatures.[6,9] LNA thiophosphoramidite monomers were generated from the correspondingly protected nucleoside alcohols[42,43] (also see supplemental material). The *in vitro* potency of the gapmers were investigated in mouse primary hepatocytes. Cells were exposed to LNAs using gymnotic conditions. *ApoB* mRNA levels were recorded at 72 h after incubation at eight different concentrations (Figure 3A). Corresponding IC_{50} values are given in Figure 3B.

The strongest target knockdown with an IC_{50} = 0.08 μM was observed for ASO-9. We therefore took this partially stereodefined hybrid design forward and used it as the starting point for the second iteration cycle. To stereochemically resolve the remaining four PS positions, all 16 possible stereoisomers were synthesized and tested for *ApoB* mRNA knockdown (Figure 4A). IC_{50} values of all possible stereoisomers are shown in Figure 4B.

Further studies executed for other target sequences lead to very similar results (Figure S4 in supplemental materials), i.e., RSSR motif in a specific position in DNA gap enhances the *in vitro* potency, which could be generalized across sequences and targets.

RNase-H-mediated mRNA knockdown *in vitro*

To assess the impact of PS_2 backbone chemistry on RNase-H-mediated target cleavage, we set up a competition assay in which an RNA-ASO heteroduplex formed with the parent compound (RTR3833) is mixed with a heteroduplex formed with a tested, PS_2-modified compound (Figure S5 in supplemental materials). The RNA in each of the heteroduplexes in a given reaction was labeled with a distinct fluorophore (FAM or Cy5) to enable independent quantification of the RNA fraction cleaved. Besides the two PS_2-modified analogs ASO-6 and ASO-26, we have also investigated a fully stereodefined version of RTR3833, namely RTR28253. This single molecule was identified in earlier studies and turned out to be the most potent *ApoB* LNA gapmer we have ever tested in our *in vitro* and *in vivo* models at that stage. RTR28253 shows the same sequence, LNA/DNA pattern, and PS stereochemistry as ASO-26 but lacking the PS_2 modifications in the flank regions, allowing a direct comparison between these two ASOs (Figure 5). Following hydrolysis with recombinant human RNase H1, we have observed no differences in cleavage extent between the parent compound and the PS_2-modified racemic analog ASO-6. However,

A

ID	Design[a]	IC_{50}[b] (μM)
ASO-12	G^C^a∨t∨t^g∨g∨t^a∨t∨T^C^A	0.13±0.01
ASO-13	G^C^a^t^t^g∨g∨t^a^t∨T^C^A	0.05±0.02
ASO-14	G^C^a^t∨t^g∨g∨t^a∨t∨T^C^A	0.12±0.02
ASO-15	G^C^a^t^t^g∨g∨t^a^t^T^C^A	0.10±0.01
ASO-16	G^C^a∨t^t^g∨g∨t^a^t^T^C^A	0.05±0.00
ASO-17	G^C^a∨t^t^g∨g∨t^a∨t∨T^C^A	0.09±0.01
ASO-18	G^C^a^t^t^g∨g∨t^a∨t^T^C^A	0.07±0.00
ASO-19	G^C^a∨t∨t^g∨g∨t^a^t∨T^C^A	0.07±0.01
ASO-20	G^C^a∨t∨t^g∨g∨t^a^t^T^C^A	0.07±0.01
ASO-21	G^C^a^t∨t^g∨g∨t^a^t∨T^C^A	0.06±0.00
ASO-22	G^C^a^t∨t^g∨g∨t^a∨t^T°C°A	0.06±0.02
ASO-23	G^C^a∨t^t^g∨g∨t^a∨t^T°C°A	0.05±0.01
ASO-24	G^C^a^t^t^g∨g∨t^a∨t∨T^C^A	0.12±0.01
ASO-25	G^C^a∨t^t^g∨g∨t^a^t∨T^C^A	0.10±0.01
ASO-26	G^C^a∨t∨t^g∨g∨t^a∨t^T^C^A	0.04±0.00
ASO-27	G^C^a^t∨t^g∨g∨t^a^t^T^C^A	0.03±0.01

B

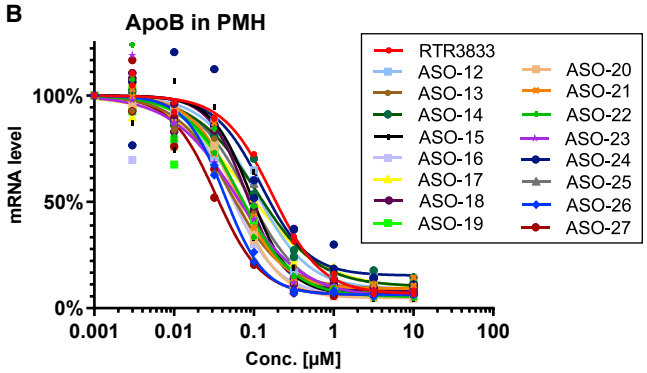

Figure 4. *In vitro ApoB* mRNA target reduction in primary hepatocytes (PMHs) after 72 h of gapmer ASOs exposure

Reduction of target *ApoB* mRNA was quantified by qRT-PCR. All experiments are carried out in triplicate. (A) Design and antisense activity are shown. Positions of PS_2 (yellow °) and stereochemistry of each phosphorothioate linkage (red ^ and green ∨) are shown. [a]Upper case designates LNA nucleotide, lower case designates DNA nucleotide, and symbols designate PS_2 (yellow °), R configuration (red ^), and S configuration (green ∨). [b]Standard deviation (±) is shown. (B) Dose-response curves for reducing *ApoB* mRNA in PMHs are shown.

when comparing the two stereodefined versions RTR28253 and ASO-26 with RTR3833, a substantially greater RNA cleavage is observed, as shown in Figure 5 (light gray bars). These data nicely demonstrate that PS_2-modified flanks have no negative impact on the mRNA cleavage rate and confirm what was reported earlier, i.e., that chirality motif, such as RSSR, as used in the design of RTR28253 and ASO-26, may well contribute to an increased RNase H activity when positioned accordingly in gapmer designs.

In vivo profiling of phosphorodithioate-modified anti-ApoB gapmers

Encouraged by the *in vitro* activities obtained, we further investigated these PS_2 ASOs *in vivo*. Therefore, animals were treated with a single dose of drug candidates and *ApoB* mRNA knockdown measured both in liver and kidney. Data points were collected after 7, 21, 28, and 42 days of drug exposure using the stereomixed ASO RTR3833 as a reference. Oligonucleotides were administered intravenously to mice at a dose level of 1 mg/kg (5 mice/group; single administration). Animals were sacrificed at 7, 21, 28, and 42 days and kidneys and livers sampled and analyzed by qPCR (Figure 6).

For the cohort of animals sacrificed 7 days post-drug administration, a target mRNA knockdown of 30% and 27% was obtained for gapmers RTR3833 and ASO-6, respectively. These two ASOs are racemic in nature and differ only in the PS_2 linkages within the flank regions. A substantially increased efficacy was observed for the stereodefined analogs, with RTR28253 showing a target knockdown of 59% and the corresponding PS_2 analog (ASO-26) showing 67% target knockdown at the same time point of analysis. For the second animal cohort sacrificed on day 21, the reference ASO RTR3833 shows only a very moderate activity of 13% target knockdown, whereas the PS_2 version ASO-6 showed a 20% reduction. For the fully stereodefined RTR28253, a 38% knockdown was observed, while the stereodefined PS_2 analog ASO-26 differentiated the most and showed still 51% of target knockdown. Twenty-eight days post-dose, the performance ranking order for the four ASOs was the same as for the other two time points. Again, a particularly strong efficacy was observed for the PS_2-stereodefined ASO-26, showing still 49% target knockdown. For the latest time point measured (42 days post-dosing), no statistically significant target knockdown was observed for all ASOs tested.

The mice experiment was conducted in accordance with the European Guidelines for the Care and Use of Laboratory Animals (directive 2010/63/EU) and was approved by the Ethical Committee for Animal Experimentation at Hoffmann-La Roche (Switzerland).

Tissue exposure and PK/PD

Drug concentrations were determined for all four ASOs at 7, 21, 28, and 42 days post-dosing both in liver and kidney. Observations from earlier studies were confirmed, where kidney exposure of the parent molecule (RTR3833) exceeded liver exposure substantially at all the time points measured. Similar profiles were obtained for the chemically modified analogs ASO-6, RTR28253, and ASO-26 as shown in Figures 7A and 7B. Overall, the organ concentrations for RTR3833 and the stereodefined version RTR28253 were almost equal for both organs. Similar profiles were also observed for the two PS_2-modified analogs ASO-6 and ASO-26, with the absolute concentrations always exceeding the exposure rates of their corresponding parent molecules. Insofar as higher tissue uptake and/or increased metabolic stability contributes to the beneficial tissue exposure remains to be investigated, but the substantially higher ASO levels observed over time for the two PS_2 analogs indicates that increased metabolic stability may indeed be a strong contributor. To address the mechanism of the enhanced tissue accumulation of PS_2 ASOs, quantitative metabolite analysis was conducted (Figure 7C). Correlating target knockdown with the actual tissue

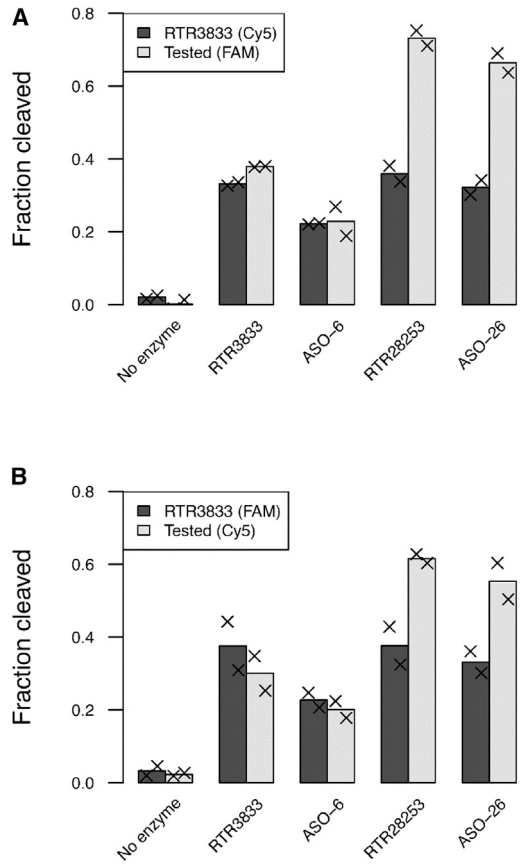

Figure 5. RNA cleavage extent in the RNase H cleavage competition assay

Fraction of RNA cleaved in each reaction for RNA hybridized with parent compound RTR3833 (dark gray) and for a tested compound (label on x axis; light gray). Left (A) and right (B) plot relate to swapped fluorophore labeling. Bars represent mean of the fractions cleaved for replicates; x symbols indicate individual observation (paired t test based on all four replicates and corrected with Holm's method: p = 0.03 for both RTR28253 and ASO-26; no significant difference between RNA cleavage extents induced by RTR3833 and ASO-6). RTR3833: G●C●a●t●t●g●g●t●a●t●T●C●A. ASO-6: G°C°a●t●t●g●g●t●a●t●T°C°A. RTR28253: G^C^a**v**t**v**t^g**v**g**v**t^a**v**t^T**v**C**v**A. ASO-26: G°C°a**v**t**v**t^g**v**g**v**t^a**v**t^T°C°A. Upper case designates LNA nucleotide, lower case designates DNA nucleotide, and symbols designate R configuration (red ^), S configuration (green **v**), PS_2 linkage (°), and phosphorothioate linkage (●).

concentration confirms the superior efficacy for the stereodefined analogs over their corresponding parents. ASO-26 and RTR28253 clearly outperform the stereomixed reference molecules RTR3833 and ASO-6.

In vivo metabolite profiling

All four candidates tested *in vivo* were further investigated with respect to ASO drug metabolism. Therefore, liver and kidney samples of the cohort sacrificed on day 7 were analyzed using an untargeted high-resolution liquid chromatography-mass spectrometry (LC-MS) approach to identify ASO metabolites and to assess their relative abundance (alternative semi-quantification). Data for the two organs are depicted as pie chart format in Figure 8.

A pronounced formation of the N-1 metabolite was found for RTR3833, resulting from the cleavage of the adenosine nucleotide from the 3′ end. Further cleavage to shorter metabolites was only seen to some extent and at small relative signal intensities in both liver and kidney. We observed a substantial improvement in metabolic stability for the PS_2 analog ASO-6, where also the N-1 fragment was detected as the main metabolite, although appearing at much lower abundancy in both organs in comparison to the stereorandom parent sequence RTR3833. Interestingly, when looking at the corresponding stereodefined analogs, the PS_2 version of RTR28253 (ASO-26) shows higher relative metabolism than the fully stereodefined gapmer, which is devoid of the PS_2 modification. N-1 fragmentation is substantially lower for both analogs compared with parent RTR3833. The main metabolite observed for both stereodefined molecules is the octamer fragment (5'-GCattggt-3').

DISCUSSION

An obvious challenge with respect to stereodefined ASOs is the fact that, with increasing length of the ASOs, the number of stereoisomers increases exponentially, leading to mixtures with 10^3–10^5 possible analogs. While the chemical synthesis of all DIs is currently not an attractive option, given the prohibitive number of compounds that would need to be prepared, researchers have focused on the synthesis of a few representatives instead.[7–10] In the context of ASO gapmers (RNase-H-mediated target knockdown), rational design elements, i.e., the 3′-SSR-triplet[10] and the RSSR-quadruplet,[44] have been reported to facilitate RNase-H-mediated target cleavage when positioned appropriately within the gap region. Having recognized the beneficial drug properties of symmetrical non-bridging PS_2, we have set out to implement the concept of reducing stereo-complexity by insertion of such achiral PS_2 linkages into the flank regions of a given lead sequence. Furthermore, when combining PS_2-modified flanks with the stereo quadruplet RSSR designed within the DNA region of gapmers, the stereo-complexity can be further reduced. For exemplification, we describe our experiments here referencing the anti-*ApoB* target ASO RTR3833. This molecule is a well-characterized LNA gapmer design based on state-of-the-art phosphoramidite chemistry, which leads to an inseparable mixture of potentially 4,096 DIs. As we demonstrated that PS_2 modifications are well tolerated in the flank regions of gapmers, we introduced two PS_2 modifications at both ends of this oligonucleotide. This reduces the number of stereocenters to eight and therefore 256 DIs. While this number might be manageable in terms of parallel synthesis capacity, we further simplified the process of identifying stereodefined single molecules, as in a classical drug discovery program, we would usually deal with several lead sequences. Exploiting the beneficial effect of chiral motifs increasing RNA knockdown efficacy, we first performed an "RSSR walk" through the gap region of our PS_2-modified lead sequence. Therefore, five ASO analogs, where the RSSR motif was placed at every possible position within the gap, were generated while keeping the remaining gap internucleoside linkages as unresolved PS. ASO-9 was identified as the most potent analog, with the RSSR motif being positioned in the center of the gap region. This partially stereodefined PS_2 hybrid was used for the second iteration cycle, where the number of DIs is further reduced to 16 from 256. It is much faster

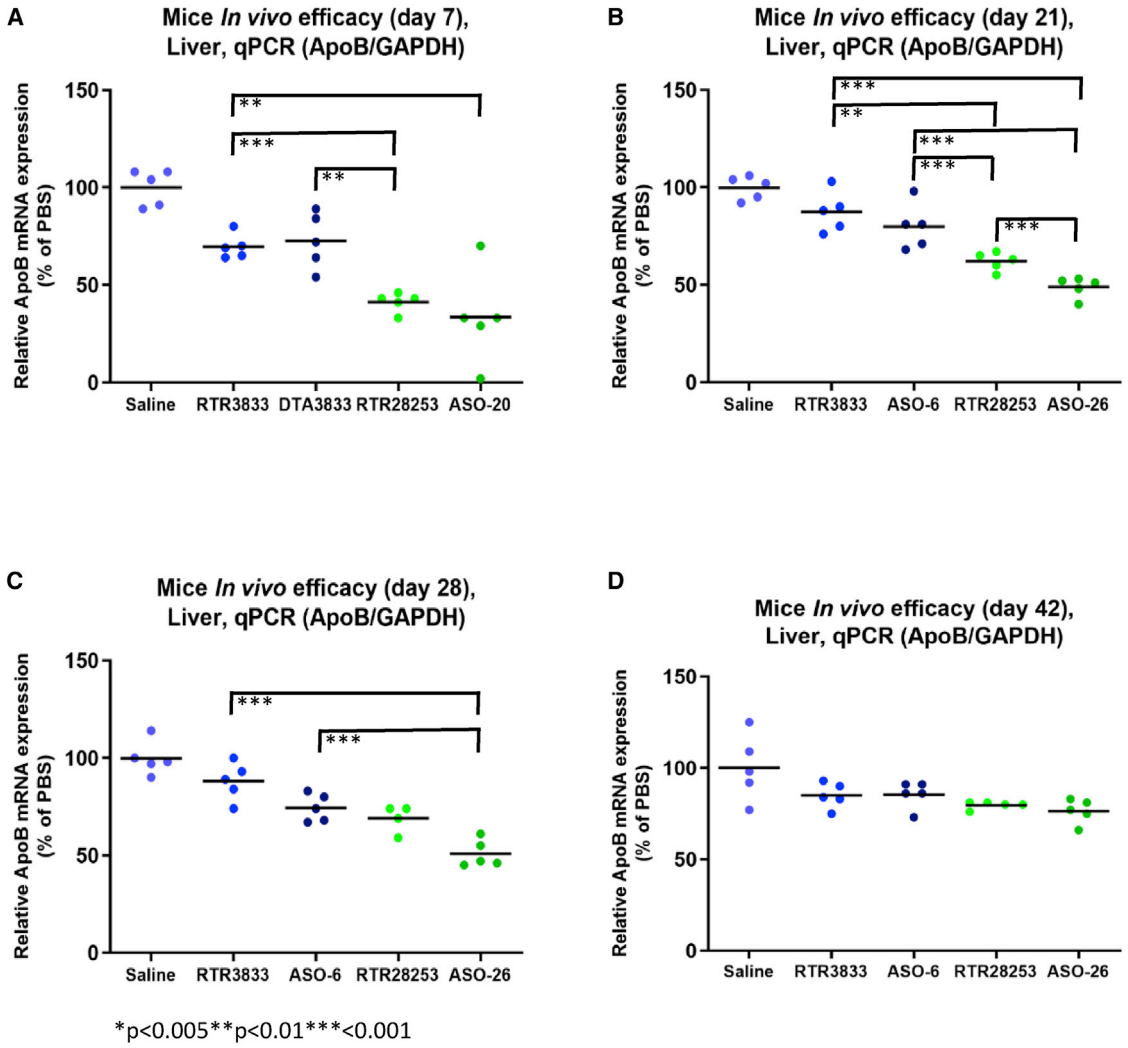

Figure 6. *In vivo* target knockdown in the liver at four different time points (day 7, 21, 28, and 42)

C57BL/6JBomTac female mice (n = 5/group) are singly dosed with 1 mg/kg by intravenous administration. Animals were sacrificed at (A) day 7, (B) day 21, (C) day 28, and (D) day 42. Livers were harvested, and reduction of target *ApoB* mRNA in the liver was quantified by qRT-PCR relative to GAPDH. One animal in cohort RTR28253/day 28 had to be anesthetized due to exaggerated pharmacology. Statistically significant (one-way ANOVA) data are indicated. **p < 0.01; ***p < 0.001.

and easier to synthesize and profile 16 ASOs than 4,096 ASOs obtained from the conventional method. These 16 single molecules were synthesized and again tested *in vitro* for *ApoB* mRNA knockdown. Compared with the parent gapmer RTR3833, which showed a potency of 0.18 μM, all stereodefined analogs identified via this strategy turned out to be equally potent or better. An approximately 5-fold increase could be obtained for the best-performing and fully stereodefined PS_2 analogs. From this set of potential candidates, ASO-26 was selected for *in vivo* profiling, not only because of its promising *in vitro* potency but rather because of the identical stereochemistry in the gap region when compared with stereodefined reference RTR28253.

In absolute terms, the stereomixed molecules (RTR3833 and ASO-6) showed ∼30% of *ApoB* mRNA knockdown while the corresponding stereodefined analogs (RTR28253 and ASO-26) performed significantly better, reducing *ApoB* mRNA by more than 50% after 7 days of drug administration. Superior efficacy of the single molecules was also confirmed for later time points (21 and 28 days post-dose), where the stereodefined PS_2 ASO-26 showed the strongest performance for all three time points measured. No significant effect was observed for the ASOs at the end of the study. When investigating ASO content in liver and kidney, the two PS_2 analogs (ASO-6 and ASO-26) show substantially higher organ exposure. Correlating ASO concentration in the liver with efficacy demonstrates again the superiority of the two stereodefined analogues versus their corresponding diastereoisomeric mixtures. How much increased metabolic stability may contribute to superior target knockdown efficacy remains to be further investigated. Nonetheless, from the metabolite

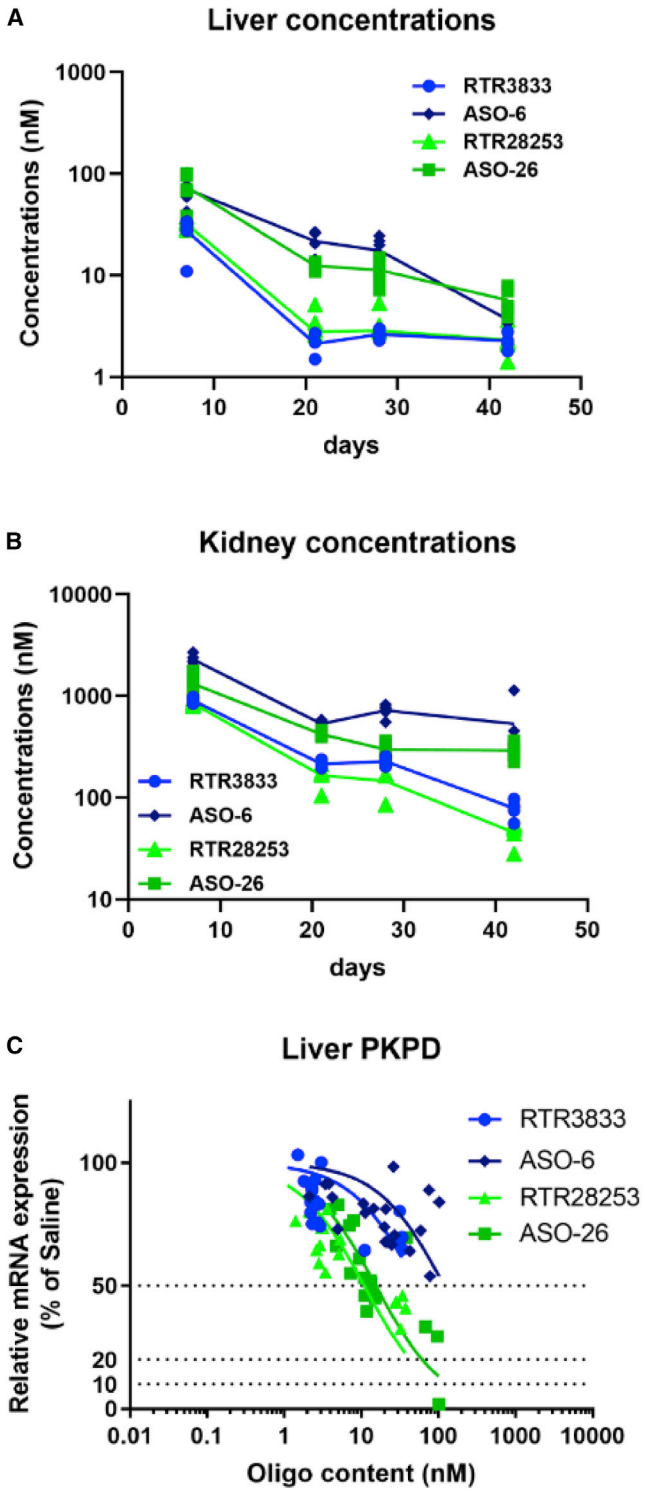

Figure 7. Tissue exposure and PK/PD

Drug concentrations measured in liver (A) and kidney (B) PK/PD relationship for all four drug candidates (C). C57BL/6JBomTac female mice (n = 5/group) are singly dosed with 1 mg/kg by intravenous administration. Animals were sacrificed at day 7, day 21, day 28, and day 42. Livers and kidneys were harvested, and ASO concentrations were measured by hELISA. y axis represents drug concentration (nM, nmols/kg tissue) in liver and kidney separately.

profiles generated, it becomes quite obvious that both PS_2 modifications as well as *S*-configured PS linkages are able to reduce metabolic degradation of a given ASO. For the diastereoisomeric mixture RTR3833, the main route of metabolism was induced by exonucleolytic degradation, as confirmed by the generation of the N-1 fragment as the major metabolite. This was clearly reduced for the PS_2 analog ASO-6, leading to a much higher overall stability. For the two stereodefined analogs, however, the main route of metabolism seems to be driven by endonucleolytic degradation, as the major metabolite for both molecules was the octamer fragment (5'-GCattggt-3'). This hypothesis is substantiated by the presence of the decamer fragment (5'-GCattggtat-3') as the second most abundant metabolite. For both fragments, the internucleoside linkages cleaved were *R* configured. As it is very well known that *R*-configured PS internucleoside linkages are more prone to enzymatic cleavage than their *S*-configured counterparts, the findings mentioned above are aligned closely to what was reported earlier.[10]

In summary, we describe herein the impact of PS_2-modified LNAs, and we propose a strategy for the identification of stereodefined gapmers that does not require the synthesis of all possible diastereomeric combinations for a given sequence. Our investigations focus on *in vitro* activity and *in vivo* efficacy as well as drug metabolism. The data clearly demonstrate superiority of stereodefined LNA gapmers over their racemic parent compounds, with the stereodefined PS_2 analog showing strongest *in vivo* performance. We have further evaluated the metabolic profile of stereodefined ASOs and confirmed the preferred metabolic cleavage for *R*-configured PS linkages *in vivo*. The *in vivo* duration of effect study data described herein strongly suggest that a combination of stereodefined internucleoside linkages with achiral PS_2 may lead to significantly superior pharmacology compared with the stereodefined or the stereomixed parent molecules. Further applications for PS_2-modified ASOs are currently under investigation and will be reported in due course.

MATERIALS AND METHODS

Oligonucleotide synthesis and purification

Oligonucleotides were synthesized using a MerMade 12 or MerMade 192 automated DNA synthesizer by Bioautomation. Syntheses were conducted on a 1-μmol scale using a controlled pore glass support (500 Å, LGC-Biosearch Technologies, UK) bearing a universal linker. Standard phosphoramidite synthesis procedures were used for unmodified LNA- and DNA-phosphoramidites (Sigma-Aldrich), i.e., 3% dichloroacetic acid in dichloromethane (CH_2Cl_2) for deblocking, 1 M 4,5-dicyanoimidazole (DCI)/0.1 M *N*-methylimidazole in acetonitrile (MeCN) as activator, 10% acetic anhydride in tetrahydrofuran (THF) and 10% *N*-methylimidazole in THF/pyridine for capping, and 0.1 M xanthane hydride in pyridine: MeCN 1:1 (v/v) for thiolation. Standard and chiral phosphoramidites were dissolved at 0.1 M

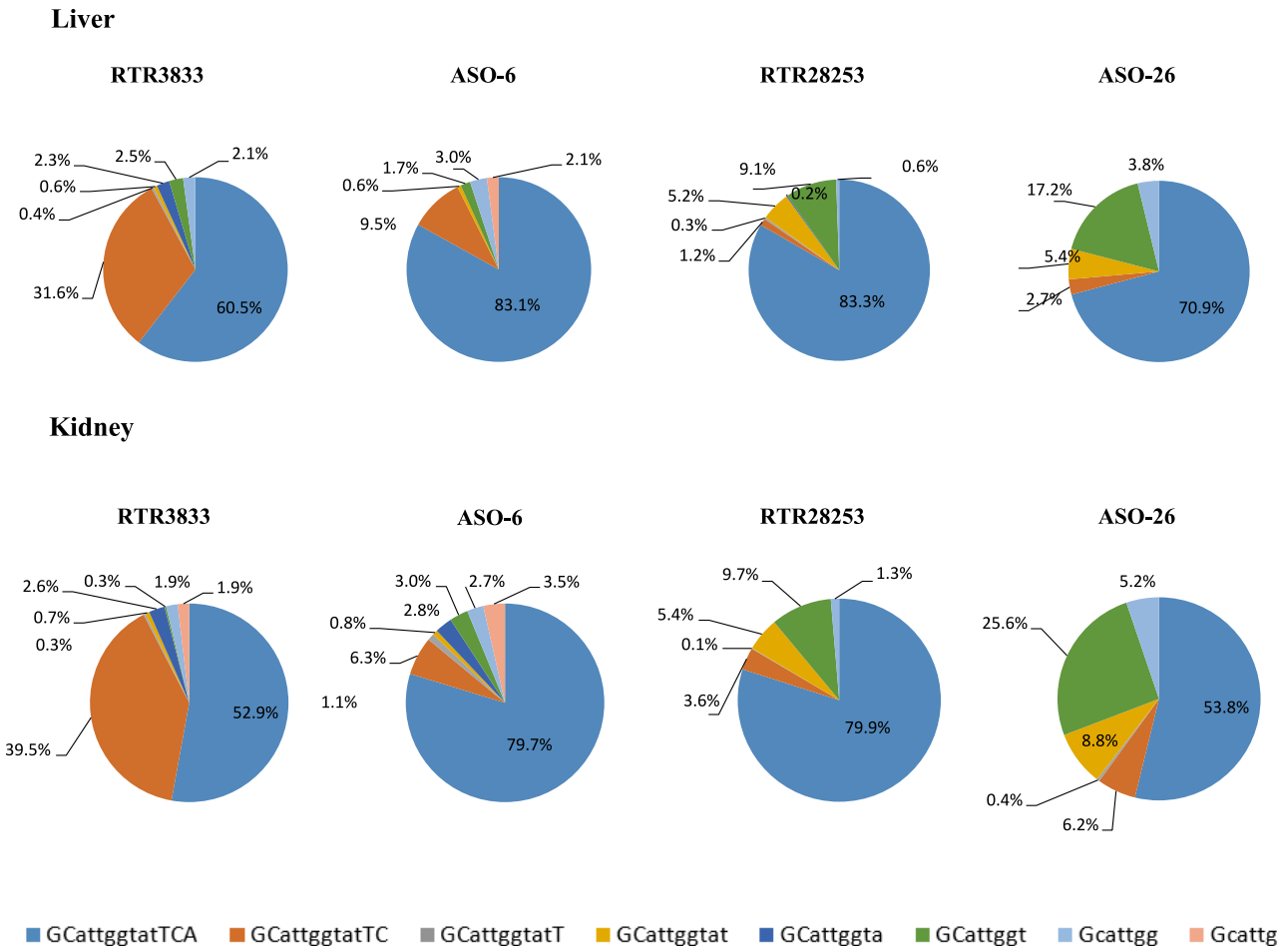

Figure 8. Metabolite formation in liver and kidney after 7 days of drug administration

C57BL/6JBomTac female mice (n = 5/group) are singly dosed with 1 mg/kg by intravenous administration. Liver and kidney were sampled at day 7. The data were measured by LC-MS/MS. Color codes represent the fragmented metabolites. RTR3833: 5′-GCatggtatTCA-3′ ASO-6: 5′-GCatggtatTCA-3′. RTR28253: 5′-GCatggtatTCA-3′. ASO-26: 5′-GCatggtatTCA-3′. Upper case designates LNA nucleotide, lower case designates DNA nucleotide, and symbols designate R configuration (red ^), S-configuration (green v), PS_2 linkage (°), and phosphorothioate linkage (●).

MeCN (+3.5% pyridine for chiral monomers) and incorporated using 3-min coupling times, while thiophosphoroamidites were prepared at 0.15 M in CH_2Cl_2: MeCN 1:9 (v/v) using 10-min coupling times. Removal of the nucleobase-protecting groups and cleavage from the solid support were achieved under standard conditions using 25% aqueous ammonia at 55°C for 12–16 h. Crude dimethoxytrityl(DMT)-on oligonucleotides were purified either using a solid-phase extraction cartridge (Oasis HLB 6 cc extraction cartridges from waters) or by preparative reverse-phase HPLC (RP-HPLC) purification (C18 column, NH_4OAc/CH_3CN buffer system) followed by DMT removal with 80% aqueous acetic acid. Following HPLC purification, oligonucleotides were desalted using HiPrep 26/10 desalting column on ÄKTA pure 25 M and lyophilized. Oligonucleotides were characterized by reversed phase ultra-performance liquid chromatography coupled to high-resolution electrospray mass spectrometry. Oligonucleotides used as capture (5'-[5bio]-[HEG]-TGAATAC-3′) and detection probe (5′-CAATGC-[HEG]-[digc63]-3') were synthesized as phosphate analogs by incorporation Biotin-CE phosphoramidite at 5′ end of LNA sequence (5'-TGAATAC-3') and conjugation with digoxigenin-NHS ester at 3′ end of LNA sequence (5'-CAATGC-3'). The labeling agents were separated by the introduction of a hexaethylene glycol (HEG) linker (Spacer-CE phosphoramidite 18).

T_m measurements

LNA gapmers and complementary RNAs were added to 10 mM phosphate buffer, 100 mM NaCl, and 0.1 nM EDTA (pH 7), resulting in a final concentration of 1.5 μM. Samples were heated to 95°C for 3 min and then slowly cooled to room temperature over a period of 30 min. Thermal melting curves were recorded at 260 nm on a Agilent Cary 3500 equipped with a Peltier Temperature Programmer using a temperature gradient that was increased by 5°C/min from 25°C to 95°C and then decreased to 25°C. The first derivatives of both curves were

used to determine the melting temperature (T_m). The values are averaged over three heating and cooling curves and are reported as value ± standard deviation.

HPLC analysis

Retention times generated for Figure 1A have been executed on an Agilent 1290 Infinity II instrument (column: Waters Acquity UPLC BEH C-18, 2.1 × 50 mm, 1.7 μM; flow: 0.8 mL/min; buffer A: 1,900 mL water/50 mL MeOH, 42 mL hexafluoroisopropanol [HFIP], 4.2 mL triethanolamine [TEA]; buffer B: 350 mL water/1,600 mL MeOH, 42 mL HFIP, 4.2 mL TEA; gradient: 0.0 min - 97% A/3% B; 0.1 min - 97% A/3% B; 22.0 min - 85% A/15% B; 30.0 min - 0% A/100% B).

Cell culture, oligonucleotide treatment, mRNA isolation, and qPCR

Hepatocytes were isolated from C57BL/6 mice by a two-step collagenase liver perfusion method as previously described. Freshly isolated primary mouse hepatocytes were plated in collagen-l-coated 96-well plates and treated in Williams Medium E containing 10% fetal bovine serum without antibiotics. Cells were treated with LNA solutions in the indicated concentrations in full cell culture medium. After an incubation time of 72 h, the cells were lysed with 125 μL PureLink Pro lysis buffer and total RNA isolated using the PureLink Pro 96 RNA Kit from Thermo Fisher according to the manufacturer's instructions. Expression *ApoB* mRNA was evaluated in a One Step RT-qPCR using Thermo Fisher TaqMan assay Mm01545150_m1 normalized to expression of Gapdh (Mm99999915_g1). All data points were performed in triplicate and IC_{50} values determined using GraphPad Prism.

RNase H cleavage competition assay

Heteroduplex RNase H substrates were prepared by mixing 20 volumes of 10× annealing buffer (200 mM Tris-HCl [pH 7.5], 200 mM KCl, 200 mM 2-mercaptoethanol, and 1 mM EDTA), two volumes of 100 μM fluorescently labeled RNA target site (5′-ACUGAAUACCAAUGCUG-3′, 5′ labeled with FAM or Cy5; manufactured by Integrated DNA Technologies), and three volumes of 100 μM ASO and 175 volumes of H_2O, followed by strand annealing in thermal cycler with a program: 2 min at 95°C, 10 min at 55°C, 10 min at 30°C, cool down to 4°C, followed by placing samples on ice. Ten microliters of the reference heteroduplex (annealed with RTR3833) was mixed with 10 μL of the tested heteroduplex (annealed with a tested compound), which was labeled with a different fluorophore. Enzymatic solution was prepared by mixing one volume of 10× RNH1-2× Mg buffer (the same composition as 10× annealing buffer supplemented with 40 mM $MgCl_2$), 8.97 volumes of H_2O, and 0.03 volumes of 0.2 mg/mL recombinant human RNase H1 isoform 2 (NP_001273763.1 preceded with glutathione [GSH] triamino acid; manufactured by Leaderna Biostructures based on a protocol kindly shared by Dr. Marcin Nowotny laboratory). Twenty microliters of the enzymatic solution were added to the mixed heteroduplexes, and the samples were incubated at 4°C for 1 min and 37°C for 10 min, followed by cooling down to 4°C. No enzyme control employed RTR3833 for both reference and tested compound. Reactions were terminated by addition of 80 μL of the stop solution (8 M urea, 1× Tris-borate-EDTA [TBE], and 5 mM EDTA). Samples were heat denatured (2 min at 95°C) and resolved on 15% polyacrylamide urea-TBE gel. Gels were visualized for FAM and Cy5 channels using iBright FL1000 Imaging System (Thermo Fisher Scientific), and bands for full length and cleaved fractions were quantified using ImageJ. The experiment was performed in triplicate for FAM-labeled reference and Cy5-labeled tested substrate and for the opposite labeling. We have observed a general trend that FAM-labeled compounds gave higher cleavage efficiency, which could be a real effect or an artifact; however, the paired t test used equal number of pairs from each labeling order (FAM-Cy5 or Cy5-FAM for reference-tested pairs), hence the impact of this confounding factor is eliminated.

Caspase activation assay

HepG2 cells were cultivated at app. 70% confluence in minimum essential medium (MEM) with GlutaMax (Gibco, no. 41090), supplemented with 10% heat-inactivated fetal calf serum. Cells were detached with 0.25% Trypsin-EDTA solution (Gibco, no. 25200056) and seeded into black, clear 96-well plates (Corning Life Sciences, no. 3904, NY, USA) at a density of 1×10^4 cells/well. Twenty-four hours post-seeding, HepG2 cells were transiently transfected with Lipofectamine 2000 (Life Technologies, no. 11668019) using 100 nM oligonucleotides dissolved in Opti-MEM (Gibco, no. 31985). Caspase 3/7 activity was determined using the Caspase-Glo 3/7 Assay (Promega, Madison, WI, USA). Reconstituted Caspase-Glo 3/7 reagent was added to the cells 24 h post-transfection, incubated for 60 min, and cell lysates were transferred into opaque 96-well plates (Corning Life Sciences, no. 3600, NY, USA) before luminescence was determined on an Enspire multi-mode plate reader (PerkinElmer) according to the manufacturer's instructions. Background readings determined from wells containing culture medium only were subtracted. Relative caspase activity was calculated as 100%× luminescence reading of a mock-treated control. All experiments were performed in triplicate.

LDH assay

LDH released into the culture media was determined using a Cytotoxicity Detection Kit (Roche 11,644,793,001, Roche Diagnostics, Roche Applied Science, Mannheim, Germany) according to the manufacturer's protocol. All experiments were performed in triplicate.

In vivo study

In vivo experiments were conducted according to the European standards, and protocols were approved by the Danish National Committee for Ethics in Animal Experiments. Inbred C57BL/6JBomTac female mice weighing 20 ± 2 g (arithmetic mean ± standard deviation) were obtained from Taconic (Denmark). The animals were housed in groups of five, and water and a standard diet were supplied *ad libitum*. The vivarium was maintained at a constant temperature (23°C ± 1°C) and humidity (40% ± 5%) under a 12 h light: 12 h dark cycle (lights on at 08:00 h) throughout the study. Mice were dosed intravenously on day 0 and anesthetized (70% CO_2 and 30%

O_2) before termination by cervical dislocation on day 7. The treatment groups (n = 5) received either 0.9% saline or saline-formulated gapmer administered by intravenous injection. At the end of the study, livers and kidneys were snap frozen for subsequent analysis.

mRNA isolation and qPCR measurements from tissue samples

Total RNA from liver and kidney was isolated using the RNeasy kit (Qiagen), and quantification of messenger RNA (mRNA) was done using TaqMan assays (Applied Biosystems). The reverse transcription reaction was carried out with random decamers, 0.5 mg total RNA, and the Moloney murine leukemia virus (M-MLV) reverse-transcriptase enzyme (Ambion) according to protocol for first-strand complementary DNA (cDNA) synthesis. Depending on expression levels, 10 ng cDNA per reaction was subsequently diluted five times in nuclease-free water before addition to the RT-PCR reaction mixture. The Applied Biosystems 7500/7900/ViiA real-time PCR instruments were used for amplification. Within each study, mRNA levels were normalized to actin, beta (Actb), or glyceraldehyde-3-phosphate dehydrogenase (Gapdh) and presented as fold changes relative to average levels in saline controls.

Quantification of intracellular LNA content by hELISA

LNA content was determined by hELISA, using a biotinylated capture probe and a digoxigenin-conjugated detection probe as described previously.[39] Sixty milligrams of tissue samples are lysed in 750 µL MagnaPure Lysis buffer. The resulted lysates were diluted and incubated with 35 nM biotinylated capture probe and 30 nM digoxigenin-coupled detection probe for 30 min at room temperature in SSCT buffer (5× saline sodium citrate buffer [SSC Buffer 20× Concentrate, Sigma-Aldrich, no. 6639] containing 0.05% Tween 20 [Sigma-Aldrich, no. P9416]) in a 96-well plate. The assembled complex is then captured on a streptavidine-coated ELISA plate (Nunc 436014) for 1 h, and after three washing steps with 2 x SSCT buffer, each well is incubated with an anti-digoxigenin-alkaline phosphatase (AP)-Fab fragment (Roche, no. 11093274910) for 1 h at room temperature. After three additional washing steps, BluePhos substrate (Kirkegaard & Perry Labs [KPL], no. 50-88-00) was added to the plates, and color development was measured spectrophotometrically at 615 nm after 20 min. For the oligo content analysis, several dilutions of each sample (50×, 100×, 200×, 400×, 800×, and 1,600×) are measured. Calculating back to the respective tissue weight and making an average of the valid values from different dilutions (i.e., the readouts within the linear range of the standard curve) generate the drug concentration.

Metabolite profiling in liver and kidney tissues

Liver and kidney tissue samples were collected from the above-described *in vivo* study and were stored at −80°C prior to analysis. To prepare tissue homogenates, 100 mg of liver or kidney tissue was placed into a CK28 tube (Precellys) and 500 µL (for liver tissue) or 300 µL (for kidney tissue) of guanidine thiocyanate (4 M in 0.1 M Tris buffer at pH 7.5) was added before mixing in the Precellys homogenizer for 10 min. The analysis of biotransformation of the oligonucleotide compounds in tissue homogenates was performed as described previously.[45,46] In brief, 50 µL of homogenate was mixed with 250 µL of guanidine thiocyanate 4 M in 0.1 M Tris buffer (pH 7.5) for 15 min at 25°C in a Thermomixer. Then 700 µL H_2O/H-FIP/DIPEA 100/2/0.2 (v/v/v) was added and mixed for 1 h at 25°C. Then the samples were centrifuged for 5 min at 14,000 rpm, and the supernatant was subjected to a solid-phase extraction (SPE) OASIS HLB 1 cc 30 mg cartridge (Waters, Wexford, Ireland) followed by the analysis with LC-MS. A Thermo Scientific Dionex UltiMate NCP-3200RS Binary Rapid Separation HPLC system was used in combination with a Pal autosampler (CTC Analytics AG, Zwingen, Switzerland) and a Thermo Scientific Orbitrap Fusion Tribrid Mass Spectrometer (Thermo Scientific, Bremen, Germany) equipped with an electrospray ionization source. The oligonucleotide metabolites were analyzed in negative ionization mode using a full-scan MS experiment combined with two parallel MS^2 experiments, one data-dependent scan, and an untargeted all-ion-fragmentation (AIF) experiment applying high collision energy. In the AIF scan, a diagnostic fragment originating from the PS backbone (O_2PS^-: m/z 94.936) was formed efficiently upon collisional activation. Based on this fragment, an accurate determination of metabolites of oligonucleotides was achieved, independent of their sequence in an untargeted but highly selective manner. MS data were analyzed using XCalibur software (Thermo Scientific, Bremen Germany). MS intensities were recorded as the sum of the most intense charge states of the most intense isotopes of the respective analyte, applying an m/z window of 5 ppm.

SUPPLEMENTAL INFORMATION

Supplemental information can be found online at https://doi.org/10.1016/j.omtn.2022.06.010.

ACKNOWLEDGMENTS

We gratefully acknowledge Heidii Mazur for her help running the *in vivo* study as well as Charlotte Øverup, Sidsel Boesen, and Christian Weile, who performed the bioanalytic analysis of *in vivo* samples. We also thank Jon Bodnar for proofreading the manuscript. This research was supported by Roche Postdoc Fellowship (RPF) program, Switzerland.

AUTHOR CONTRIBUTIONS

J.D. and M.L. designed and performed experiments, analyzed data, and wrote the manuscript. A.S. supported oligo synthesis. M.D. performed the *in vitro* evaluation experiments and analyzed data. K.J. and M.R.M. performed the *in vivo* study. S. Schmidt and H.N. performed *in vitro* evaluation experiments and analyzed data, analyzed the *in vivo* data, and reviewed and edited the manuscript. T.M. performed caspase induction experiment. S. Sewing analyzed the caspase data and reviewed and edited the paper. C.H. performed *in vitro* metabolic stability experiment and *in vivo* metabolite identification study and analyzed data. S. Schadt and A.B. analyzed *in vitro* metabolic stability and *in vivo* metabolite identification data and reviewed and edited the manuscript. L.J.K. performed RNase H cleavage competition assay, analyzed data, and reviewed and edited the manuscript. E.K. coordinated *in vivo* study and reviewed and edited the

manuscript. E.F. provided valuable historical data and advice. T.K. and J.W. provided support to the paper. K.B. conceived the project idea, supervised the work, and wrote the manuscript.

DECLARATION OF INTERESTS

J.D. is a member of a shareholder group with pooled voting rights of Roche as well as one of their representatives on the board of directors. J.W. is an academic collaborator. All the rest of the authors are or were employees of F. Hoffmann-La Roche AG.

REFERENCES

1. Nguyen, L.A., He, H., and Pham-Huy, C. (2006). Chiral drugs: an overview. Int. J. Biomed. Sci. *2*, 85–100.
2. Hagedorn, P.H., Persson, R., Funder, E.D., Albaek, N., Diemer, S.L., Hansen, D.J., Moller, M.R., Papargyri, N., Christiansen, H., Hansen, B.R., et al. (2018). Locked nucleic acid: modality, diversity, and drug discovery. Drug Discov. Today *23*, 101–114.
3. Stec, W.J., Grajkowski, A., Koziolkiewicz, M., and Uznanski, B. (1991). Novel route to oligo(deoxyribonucleoside phosphorothioates). Stereocontrolled synthesis of P-chiral oligo(deoxyribonucleoside phosphorothioates). Nucleic Acids Res. *19*, 5883–5888.
4. Guga, P., and Stec, W.J. (2003). Synthesis of phosphorothioate oligonucleotides with stereodefined phosphorothioate linkages. Curr. Protoc. Nucleic Acid Chem. *Chapter 4*, Unit 4.17.
5. Knouse, K.W., DeGruyter, J.N., Schmidt, M.A., Zheng, B., Vantourout, J.C., Kingston, C., Mercer, S.E., Mcdonald, I.M., Olson, R.E., Zhu, Y., et al. (2018). Unlocking P(V): reagents for chiral phosphorothioate synthesis. Science *361*, 1234–1238.
6. Oka, N., Yamamoto, M., Sato, T., and Wada, T. (2008). Solid-phase synthesis of stereoregular oligodeoxyribonucleoside phosphorothioates using bicyclic oxazaphospholidine derivatives as monomer units. J. Am. Chem. Soc. *130*, 16031–16037.
7. Li, M., Lightfoot, H.L., Halloy, F., Malinowska, A.L., Berk, C., Behera, A., Schumperli, D., and Hall, J. (2017). Synthesis and cellular activity of stereochemically-pure 2'-O-(2-methoxyethyl)-phosphorothioate oligonucleotides. Chem. Commun. (Camb.) *53*, 541–544.
8. Ostergaard, M.E., De Hoyos, C.L., Wan, W.B., Shen, W., Low, A., Berdeja, A., Vasquez, G., Murray, S., Migawa, M.T., Liang, X.H., et al. (2020). Understanding the effect of controlling phosphorothioate chirality in the DNA gap on the potency and safety of gapmer antisense oligonucleotides. Nucleic Acids Res. *48*, 1691–1700.
9. Wan, W.B., Migawa, M.T., Vasquez, G., Murray, H.M., Nichols, J.G., Gaus, H., Berdeja, A., Lee, S., Hart, C.E., Lima, W.F., et al. (2014). Synthesis, biophysical properties and biological activity of second generation antisense oligonucleotides containing chiral phosphorothioate linkages. Nucleic Acids Res. *42*, 13456–13468.
10. Iwamoto, N., Butler, D.C.D., Svrzikapa, N., Mohapatra, S., Zlatev, I., Sah, D.W.Y., Meena Standley, S.M., Lu, G., Apponi, L.H., et al. (2017). Control of phosphorothioate stereochemistry substantially increases the efficacy of antisense oligonucleotides. Nat. Biotechnol. *35*, 845–851.
11. Duschmale, J., Hansen, H.F., Duschmale, M., Koller, E., Albaek, N., Moller, M.R., Jensen, K., Koch, T., Wengel, J., and Bleicher, K. (2020). *In vitro* and *in vivo* properties of therapeutic oligonucleotides containing non-chiral 3' and 5' thiophosphate linkages. Nucleic Acids Res. *48*, 63–74.
12. Brill, W.K.D., Nielsen, J., and Caruthers, M.H. (1991). Synthesis of deoxydinucleoside phosphorodithioates. J. Am. Chem. Soc. *113*, 3972–3980.
13. Brill, W.K.D., Tang, J.Y., Ma, Y.X., and Caruthers, M.H. (1989). Synthesis of oligodeoxynucleoside phosphorodithioates via thioamidites. J. Am. Chem. Soc. *111*, 2321–2322.
14. Caruthers, M.H., Beaton, G., Cummins, L., Dellinger, D., Graff, D., Ma, Y.X., Marshall, W.S., Sasmor, H., Shankland, P., Van Wu, J., et al. (1991). Chemical and biochemical studies with dithioate DNA. Nucleosides Nucleotides *10*, 47–59.
15. Tonkinson, J.L., Guvakova, M., Khaled, Z., Lee, J., Yakubov, L., Marshall, W.S., Caruthers, M.H., and Stein, C.A. (1994). Cellular pharmacology and protein binding of phosphoromonothioate and phosphorodithioate oligodeoxynucleotides: a comparative study. Antisense Res. Dev. *4*, 269–278.
16. Cummins, L., Graff, D., Beaton, G., Marshall, W.S., and Caruthers, M.H. (1996). Biochemical and physicochemical properties of phosphorodithioate DNA. Biochemistry *35*, 8734–8741.
17. Vaughn, J.P., Stekler, J., Demirdji, S., Mills, J.K., Caruthers, M.H., Iglehart, J.D., and Marks, J.R. (1996). Inhibition of the erbB-2 tyrosine kinase receptor in breast cancer cells by phosphoromonothioate and phosphorodithioate antisense oligonucleotides. Nucleic Acids Res. *24*, 4558–4564.
18. Wiesler, W.T., and Caruthers, M.H. (1996). Synthesis of phosphorodithioate DNA via sulfur-linked, base-labile protecting groups(1). J. Org. Chem. *61*, 4272–4281.
19. Cheng, X., DeLong, R.K., Wickstrom, E., Kligshteyn, M., Demirdji, S.H., Caruthers, M.H., and Juliano, R.L. (1997). Interactions between single-stranded DNA binding protein and oligonucleotide analogs with different backbone chemistries. J. Mol. Recognit. *10*, 101–107.
20. Grandas, A., Marshall, W.S., Nielsen, J., and Caruthers, M.H. (1989). Synthesis of deoxycytidine oligomers containing phosphorodithioate linkages. Tetrahedron Lett. *30*, 543–546.
21. Bjergarde, K., and Dahl, O. (1991). Solid phase synthesis of oligodeoxyribonucleoside phosphorodithioates from thiophosphoramidites. Nucleic Acids Res. *19*, 5843–5850.
22. Capaldi, D.C., Cole, D.L., and Ravikumar, V.T. (2000). Highly efficient solid phase synthesis of oligonucleotide analogs containing phosphorodithioate linkages. Nucleic Acids Res. *28*, E40.
23. Li, N.S., Frederiksen, J.K., and Piccirilli, J.A. (2012). Automated solid-phase synthesis of RNA oligonucleotides containing a nonbridging phosphorodithioate linkage via phosphorothioamidites. J. Org. Chem. *77*, 9889–9892.
24. Yang, X. (2016). Solid-phase synthesis of oligodeoxynucleotide analogs containing phosphorodithioate linkages. Curr. Protoc. Nucleic Acid Chem. *66*, 4–71. 1–4.71.14.
25. Yang, X. (2017). Solid-phase synthesis of RNA analogs containing phosphorodithioate linkages. Curr. Protoc. Nucleic Acid Chem. *70*, 4–77. 1–4.77.13.
26. Jaroszewski, J.W., Clausen, V., Cohen, J.S., and Dahl, O. (1996). NMR investigations of duplex stability of phosphorothioate and phosphorodithioate DNA analogues modified in both strands. Nucleic Acids Res. *24*, 829–834.
27. Furrer, P., Billeci, T.M., Donati, A., Kojima, C., Karwowski, B., Sierzchala, A., Stec, W., and James, T.L. (1999). Structural effect of complete [Rp]-phosphorothioate and phosphorodithioate substitutions in the DNA strand of a model antisense inhibitor-target RNA complex. J. Mol. Biol. *285*, 1609–1622.
28. Krieg, A.M., Matson, S., and Fisher, E. (1996). Oligodeoxynucleotide modifications determine the magnitude of B cell stimulation by CpG motifs. Antisense Nucleic Acid Drug Dev. *6*, 133–139.
29. Yang, X., Sierant, M., Janicka, M., Peczek, L., Martinez, C., Hassell, T., Li, N., Li, X., Wang, T., and Nawrot, B. (2012). Gene silencing activity of siRNA molecules containing phosphorodithioate substitutions. ACS Chem. Biol. *7*, 1214–1220.
30. Pallan, P.S., Yang, X., Sierant, M., Abeydeera, N.D., Hassell, T., Martinez, C., Janicka, M., Nawrot, B., and Egli, M. (2014). Crystal structure, stability and Ago2 affinity of phosphorodithioate-modified RNAs. RSC Adv. *4*, 64901–64904.
31. Wu, S.Y., Yang, X., Gharpure, K.M., Hatakeyama, H., Egli, M., McGuire, M.H., Nagaraja, A.S., Miyake, T.M., Rupaimoole, R., Pecot, C.V., et al. (2014). 2′-OMe-phosphorodithioate-modified siRNAs show increased loading into the RISC complex and enhanced anti-tumour activity. Nat. Commun. *5*, 3459.
32. Yang, X., Fennewald, S., Luxon, B.A., Aronson, J., Herzog, N.K., and Gorenstein, D.G. (1999). Aptamers containing thymidine 3'-O-phosphorodithioates: synthesis and binding to nuclear factor-kappaB. Bioorg. Med. Chem. Lett. *9*, 3357–3362.
33. Yang, X., Bassett, S.E., Li, X., Luxon, B.A., Herzog, N.K., Shope, R.E., Aronson, J., Prow, T.W., Leary, J.F., Kirby, R., et al. (2002). Construction and selection of bead--bound combinatorial oligonucleoside phosphorothioate and phosphorodithioate aptamer libraries designed for rapid PCR-based sequencing. Nucleic Acids Res. *30*, e132.
34. Abeydeera, N.D., Egli, M., Cox, N., Mercier, K., Conde, J.N., Pallan, P.S., Mizurini, D.M., Sierant, M., Hibti, F.E., Hassell, T., et al. (2016). Evoking picomolar binding in RNA by a single phosphorodithioate linkage. Nucleic Acids Res. *44*, 8052–8064.
35. Yang, X., Dinuka Abeydeera, N., Liu, F.W., and Egli, M. (2017). Origins of the enhanced affinity of RNA–protein interactions triggered by RNA phosphorodithioate backbone modification. Chem. Commun. (Camb.) *53*, 10508–10511.

36. Dolot, R., Lam, C.H., Sierant, M., Zhao, Q., Liu, F.W., Nawrot, B., Egli, M., and Yang, X. (2018). Crystal structures of thrombin in complex with chemically modified thrombin DNA aptamers reveal the origins of enhanced affinity. Nucleic Acids Res. *46*, 4819–4830.

37. Ghosh, M.K., Ghosh, K., Dahl, O., and Cohen, J.S. (1993). Evaluation of some properties of a phosphorodithioate oligodeoxyribonucleotide for antisense application. Nucleic Acids Res. *21*, 5761–5766.

38. Okruszek, A., Sierzcha-La, A., Fearon, K.L., and Stec, W.J. (1995). Synthesis of oligo(-deoxyribonucleoside phosphorodithioate)s by the dithiaphospholane approach. J. Org. Chem. *60*, 6998–7005.

39. Straarup, E.M., Fisker, N., Hedtjärn, M., Lindholm, M.W., Rosenbohm, C., Aarup, V., Hansen, H.F., Ørum, H., Hansen, J.B., and Koch, T. (2010). Short locked nucleic acid antisense oligonucleotides potently reduce apolipoprotein B mRNA and serum cholesterol in mice and non-human primates. Nucleic Acids Res. *38*, 7100–7111.

40. Sewing, S., Boess, F., Moisan, A., Bertinetti-Lapatki, C., Minz, T., Hedtjaern, M., Tessier, Y., Schuler, F., Singer, T., and Roth, A.B. (2016). Establishment of a predictive *in vitro* assay for assessment of the hepatotoxic potential of oligonucleotide drugs. PLoS One *11*, e0159431.

41. Seth, P.P., and Swayze, E.E. (2019). The medicinal chemistry of RNase H-activating antisense oligonucleotides. In Advances in Nucleic Acid Therapeutics, S. Agrawal and M.J. Gait, eds. (The Royal Society of Chemistry), pp. 32–61.

42. Bleicher, K., Duschmale, J., Duschmale, M.B., Hansen, H.F., Funder, E., Koch, T., Li, M., Schaeublin, A., Shu, X., and Wu, Y. (2019). Gapmer Oligonucleotides Comprising a Phosphorodithioate Internucleoside Linkage. WO 2019122282 A1.

43. Bleicher, K., Duschmale, J., Duschmale, M.B., Hansen, H.F., Koch, T., Li, M., Schaeublin, A., Shu, X., and Wu, Y. (2019). Novel Thiophosphoramidites. WO 2019122277 A1.

44. Bleicher, K., Hansen, H.F., Koch, T., Albaek, N., and Funder, E.D. (2019). Methods for Identifying Improved Stereodefined Phosphorothioate Oligonucleotide Variants of Antisense Oligonucleotides Utilising Sub-libraries of Partially Stereodefined Oligonucleotides. WO 2019073018 A1.

45. Husser, C., Brink, A., Zell, M., Muller, M.B., Koller, E., and Schadt, S. (2017). Identification of GalNAc-conjugated antisense oligonucleotide metabolites using an untargeted and generic approach based on high resolution mass spectrometry. Anal. Chem. *89*, 6821–6826.

46. Husser, C., Koller, E., Brink, A., and Schadt, S. (2019). Studying the biotransformation of phosphorothioate-containing oligonucleotide drugs by LC-MS. Methods Mol. Biol. *2036*, 307–315.

OMTN, Volume *29*

Supplemental information

Investigating discovery strategies and pharmacological properties of stereodefined phosphorodithioate LNA gapmers

Jörg Duschmalé, Adrian Schäublin, Erik Funder, Steffen Schmidt, Łukasz J. Kiełpiński, Helle Nymark, Klaus Jensen, Troels Koch, Martina Duschmalé, Erich Koller, Marianne Ravn Møller, Simone Schadt, Christophe Husser, Andreas Brink, Sabine Sewing, Tanja Minz, Jesper Wengel, Konrad Bleicher, and Meiling Li

LNA thiophosphoramidite monomer synthesis:

S-(2-sulfanylethyl) benzenecarbothioate

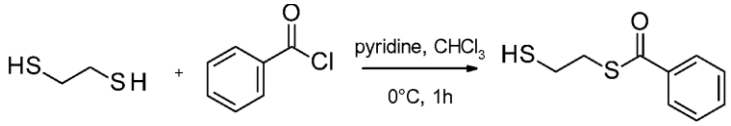

To a solution of 1,2-ethanedithiol (133.6 mL, 1592 mmol, 1 eq) and pyridine (64.4 mL, 796 mmol, 0.5 eq) in chloroform (200 mL) was added benzoyl chloride (92.4 mL, 796 mmol, 0.5 eq) in chloroform (200 mL) dropwise for 1 hr, and the reaction was stirred at 0 °C for 1 hr. The mixture was washed with water (300 mL) and brine (300 mL). The organic phase was dried over Na_2SO_4 and concentrated to a yellow oil. The oil was distilled (135~145 °C) to afford S-(2-sulfanylethyl) benzenecarbothioate (40 g, 202 mmol, 13% yield) as a colorless oil. ^{1}H NMR (400 MHz, $CDCl_3$) δ 7.97 (d, *J* = 7.34 Hz, 2H), 7.53-7.64 (m, 1H), 7.47 (t, *J* = 7.58 Hz, 2H), 3.31 (t, *J* = 7.34 Hz, 2H), 2.77-2.86 (m, 2H), 1.70 (t, *J* = 8.56 Hz, 1H).

S-[2-[[(1R,3R,4R,7S)-l-[[bis(4-methoxyphenyl)-phenyl-methoxy] methyl]-3-(5-[2-methyl-2,4-dioxo-pyrimidin-l-yl)-2,5-dioxabicyclo[2.2.1]heptan-7-yl]oxy-pyrrolidin-1-yl-phosphanyl] sulfanylethyl] benzenecarbothioate

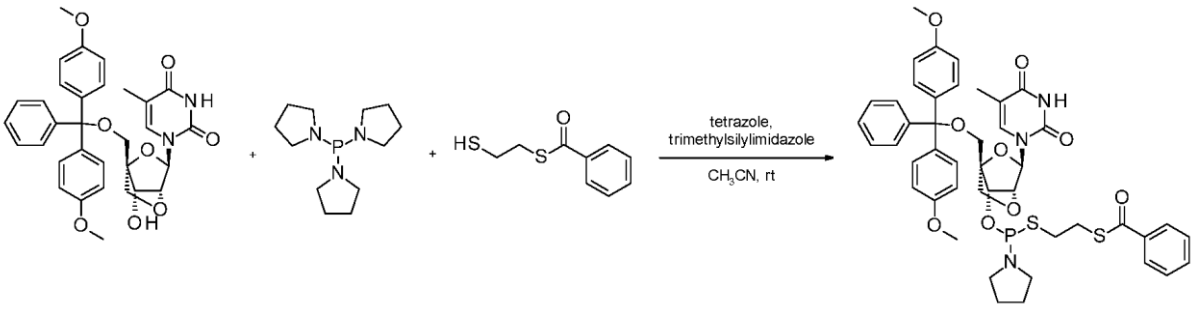

1-[(1R,4R,6R,7S)-4-[[bis(4-methoxyphenyl)-phenyl-methoxy]methyl]-7-hydroxy-2,5-dioxabicyclo[2.2.1]heptan-6-yl]-5-methyl-pyrimidine-2,4-dione (2.29 g, 4.00 mmol, 1.0 eq) was dissolved in 60 mL of anhydrous dichloromethane to which a spatula of 3 Å molecular sieves was added. Tripyrrolidin-1-ylphosphane (960 mg, 3.98 mmol, 0.99 eq) was added via syringe followed by seven 0.1 mmol aliquots of tetrazole (7 x 0.4 mL of a 0.5 M solution in

anhydrous acetonitrile stored over 3 Å molecular sieves) at 2 min intervals. N-trimethylsilylimidazole (56.0 mg, 0.400 mmol, 0.1 eq) was then added to the reaction. After 5 min, tetrazole (21.6 mL of a 0.5 M solution in anhydrous acetonitrile) was added, immediately followed by the addition of S-(2-sulfanylethyl) benzenecarbothioate (1.04 g, 5.24 mmol, 1.31 eq). The reaction was allowed to proceed for 120 sec. Four identical batches of the reaction were combined and quenched by pouring the solution into 600 mL of dichloromethane containing 40 mL of triethylamine. The mixture was immediately washed with saturated sodium bicarbonate (800 mL) followed by 10% sodium carbonate (2 x 800 mL) and brine (800 mL). The organic layer was dried over Na_2SO_4. After 10-15 min the drying agent was removed by filtration. Triethylamine (40 mL) was added to the solution which was concentrated using a rotary evaporator to a syrup. The syrup was dissolved in toluene (200 mL) and triethylamine (40 mL), and this solution was pipetted into 4500 mL of vigorously stirred heptane to precipitate the fluffy white product. After most of the heptane was decanted, the white precipitate was collected by filtration through a medium sintered glass funnel and subsequently dried under vacuum to give a white solid. The solid was purified by prep-HPLC (Phenomenex Gemini C18, 250x50 mm, 10 mm column, 0.05% ammonium hydroxide in water / CH_3CN), and freeze-dried to afford 4.58 g of target compound as a white solid. ^{31}P NMR (162 MHz, CD_3CN) δ 167.6, 164.2. ^{1}H NMR (400 MHz, CD_3CN) δ 9.16 (br s, 1H), 7.93 (t, *J* = 7.41 Hz, 2H), 7.60-7.71 (m, 1H), 7.45-7.57 (m, 4H), 7.24-7.45 (m, 7H), 6.90 (d, *J* = 8.93 Hz, 4H), 5.53-5.63 (m, 1H), 4.41-4.64 (m, 2H), 3.74-3.88 (m, 8H), 3.39-3.63 (m, 2H), 3.03-3.32 (m, 5H), 2.77-2.94 (m, 2H), 1.66-1.84 (m, 4H), 1.54-1.66 (m, 3H).

S-[2-[[(1R,3R,4R,7 S)-3-(6-benzamidopurin-9-yl)- 1- [[bis(4-methoxyphenyl)-phenyl-methoxy] methyl]-2,5-dioxabicyclo-[2.2.1]-heptan-7-yl]oxy-pyrrolidin-1-ylphosphanyljsulfanylethyl]benzenecarbothioate

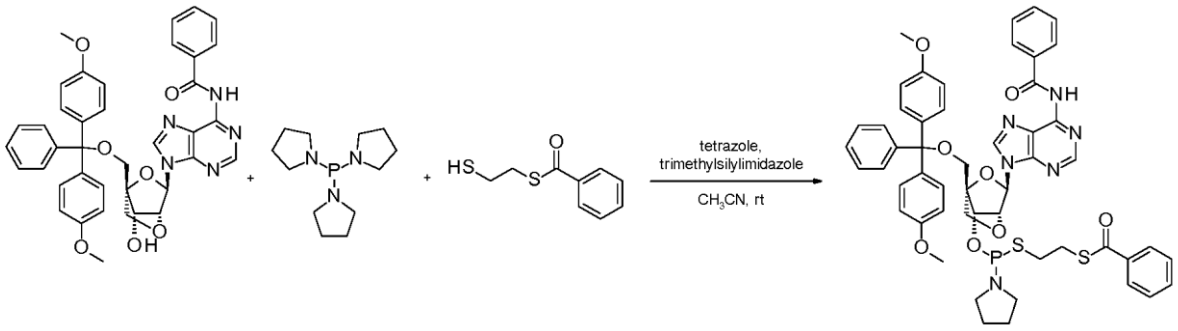

N-[9-[(1R,4R,6R,7S)-4-[[bis(4-methoxyphenyl)-phenyl-methoxy]methyl]-7-hydroxy-2,5-dioxabicyclo[2.2.1]heptan-6-yl]purin-6-yl]benzamide (2.74 g, 4.00 mmol, 1.0 eq) was dissolved in 60 mL of anhydrous dichloromethane to which a spatula of 3 Å molecular sieves was added. Tripyrrolidin-1-ylphosphane (960 mg, 3.98 mmol, 0.99 eq) was added via syringe followed by seven 0.1 mmol aliquots of tetrazole (7 * 0.4 mL of a 0.5 M solution in anhydrous acetonitrile stored over 3 Å molecular sieves) at 2 min intervals. 1-(trimethylsilyl)-1H-imidazole (56.0 mg, 0.400 mmol, 0.1 eq) was then added to the reaction. After 5 min, tetrazole (21.6 mL of a 0.5 M solution in anhydrous acetonitrile) was added, immediately followed by the addition of S-(2-sulfanylethyl) benzenecarbothioate (1.04 g, 5.24 mmol, 1.31 eq). The reaction was allowed to proceed for 120 s. Four identical batches of the reaction were united and quenched by pouring the solution into 600 mL of dichloromethane containing 40 mL of triethylamine. The mixture was immediately washed with saturated sodium bicarbonate (800 mL) followed by 10% sodium carbonate (2 x 800 mL) and brine (800 mL). The organic layer was dried over Na_2SO_4. After 10-15 mins the drying agent was removed by filtration. Triethylamine (10 mL) was added to the solution which was concentrated using a rotary evaporator to a syrup. The syrup was dissolved in toluene (100 mL) and triethylamine (20 mL), and this solution was pipetted into 4500 mL of vigorously stirred heptane to precipitate the fluffy white product. After most of the heptane was decanted, the white precipitate was collected by filtration through a medium sintered glass funnel and subsequently dried under vacuum to give a white solid. The solid was purified by prep-HPLC (Phenomenex Gemini C18,

250x50 mm, 10 mm column, 0.05% ammonium hydroxide in water / CH_3CN), and freeze-dried to afford 5.26 g of target compound as a white solid. ^{31}P NMR (162 MHz, CD_3CN) d 165.6, 164.7. ^{1}H NMR (400 MHz, CD_3CN) δ 8.56 (d, *J* = 10.76 Hz, 1H), 8.24 (d, *J* = 10.27 Hz, 1H), 7.82-7.93 (m, 2H), 7.71-7.80 (m, 2H), 6.92-7.54 (m, 14H), 6.68-6.83 (m, 4H), 6.03 (d, *J* = 6.48 Hz, 1H), 4.70-4.90 (m, 2H), 3.81-3.98 (m, 2H), 3.59-3.68 (m, 7H), 3.25-3.47 (m, 2H), 2.81-3.02 (m, 6H), 2.56-2.81 (m, 2H), 1.44-1.72 (m, 4H).

S-[2-[[(1R,3R,4R,7 S)-3-(4-benzamido-5-methyl-2-oxo-pyrimidin-1-yl)-1-[[bis(4 methoxyphenyl)-phenyl-methoxy] methyl] -2,5-dioxabicyclo [2.2.1] heptan-7-yl] oxypyrrolidin-1-yl-phosphanyl] sulfanylethyl] benzenecarbothioate

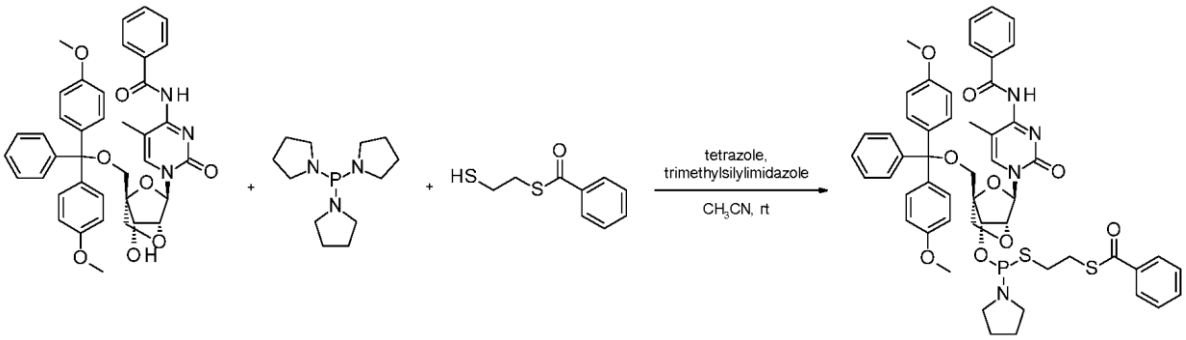

N-[1-[(1R,4R,6R,7S)-4-[[bis(4-methoxyphenyl)-phenyl-methoxy]methyl]-7-hydroxy-2,5-dioxabicyclo[2.2.1]heptan-6-yl]-5-methyl-2-oxo-pyrimidin-4-yl]benzamide (2.70 g, 4.00 mmol, 1.0 eq) was dissolved in 60 mL of anhydrous dichloromethane to which a spatula of 3 Å molecular sieves was added. Tripyrrolidin-1-ylphosphane (965 mg, 4.00 mmol, 1.0 eq) was added via syringe followed by seven 0.1 mmol aliquots of tetrazole (7 x 0.4 mL of a 0.5 M solution in anhydrous acetonitrile stored over 3 Å molecular sieves) at 2 min intervals. 1-(trimethylsilyl)-1H-imidazole (56.0 mg, 0.400 mmol, 0.1 eq) was then added to the reaction. After 5 min, tetrazole (21.6 mL of a 0.5 M solution in anhydrous acetonitrile) was added, immediately followed by the addition of S-(2-sulfanylethyl) benzenecarbothioate (1.04 g, 5.24 mmol, 1.31 eq). The reaction was allowed to proceed for 120 sec. Four identical batches of the reaction were quenched and united by pouring the solution into 600 mL of dichloromethane

containing 40 mL of triethylamine. The mixture was immediately washed with saturated sodium bicarbonate (800 mL) followed by 10% sodium carbonate (2 x 800 mL) and brine (800 mL). The organic layer was dried over Na_2SO_4. After 10-15 min the drying agent was removed by filtration. Triethylamine (40 mL) was added to the solution which was concentrated using a rotary evaporator to a syrup. The syrup was dissolved in toluene (100 mL) and triethylamine (30 mL), and this solution was pipetted into 4500 mL of vigorously stirred heptane to precipitate the fluffy white product. After most of the heptane was decanted, the white precipitate was collected by filtration through a medium sintered glass funnel and subsequently dried under vacuum to give a white solid. The solid was purified by prep-HPLC (Phenomenex Gemini C18, 250x50mm, 10 mm column, 0.05% ammonium hydroxide in water / CH_3CN) and freeze-dried to afford 2.05 g of target compound as a white solid. ^{31}P NMR (162 MHz, CD_3CN) δ 171.2, 167.4. ^{1}H NMR (400 MHz, CD_3CN) δ 8.18-8.32 (m, 2H), 7.81-7.93 (m, 3H), 7.35-7.60 (m, 14H), 7.17-7.35 (m, 2H), 6.93 (d, *J* = 8.93 Hz, 4H), 5.65 (d, *J* = 15.04 Hz, 1H), 4.56-4.72 (m, 2H), 3.69-3.90 (m, 8H), 3.45-3.61 (m, 2H), 3.03-3.26 (m, 6H), 2.76-3.02 (m, 2H), 1.65-1.93 (m, 7H).

S-[2-[[(lR,3R,4R,7S)-l-[[bis(4-methoxyphenyl)-phenyl-methoxy]methyl]-3-[2-[(E)-dimethylaminomethyleneamino]-6-oxo-lH-purin-9-yl]-2,5-dioxabicyclo[2.2.1]heptan-7-yl]oxy-pyrrolidin-l-yl-phosphanyl]sulfanylethyl] benzenecarbothioate

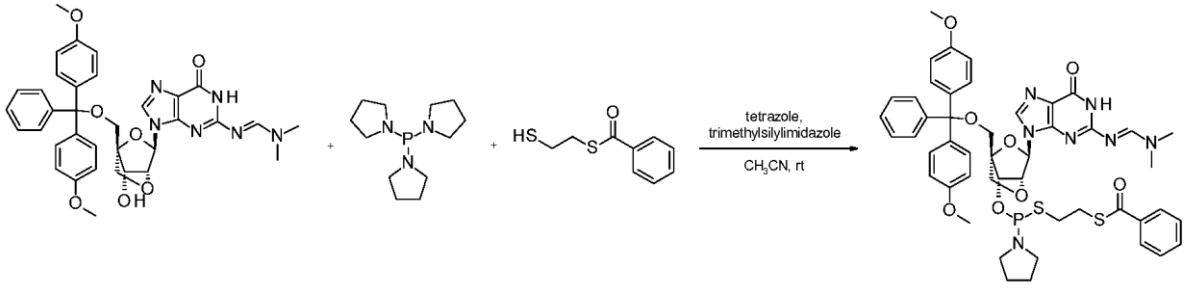

N'-[9-[(1R,4R,6R,7S)-4-[[bis(4-methoxyphenyl)-phenyl-methoxy]methyl]-7-hydroxy-2,5-dioxabicyclo[2.2.1]heptan-6-yl]-6-oxo-1H-purin-2-yl]-N,N-dimethyl-formamidine (2.62 mg, 4.00 mmol, 1.0 eq) was dissolved in 200 mL of anhydrous dichloromethane to which a spatula of 3 Å molecular sieves was added. Tripyrrolidin-1-ylphosphane (965 mg, 4.00 mmol, 1.0 eq) was added via syringe followed by seven 0.1 mmol aliquots of tetrazole (7 x 0.4 mL of a 0.5 M solution in anhydrous acetonitrile stored over 3 Å molecular sieves) at 2 min intervals. 1-(trimethylsilyl)-1H-imidazole (56.0 mg, 0.400 mmol, 0.1 eq) was then added to the reaction. After 5 min, tetrazole (21.6 mL of a 0.5 M solution in anhydrous acetonitrile) was added, immediately followed by the addition of S-(2-sulfanylethyl) benzenecarbothioate (1.04 g, 5.24 mmol, 1.31 eq). The reaction was allowed to proceed for 180 s.

Four identical batches were combined and quenched by pouring the solutions into 600 mL of dichloromethane containing 40 mL of triethylamine. The mixture was immediately washed with saturated sodium bicarbonate (800 mL) followed by 10% sodium carbonate (2 * 800 mL) and brine (800 mL). The organic layer was dried over Na_2SO_4. After 10-15 min the drying agent was removed by filtration. Triethylamine (40 mL) was added to the solution which was concentrated using a rotary evaporator to a syrup. The syrup was dissolved in toluene (100 mL) and triethylamine (30 mL), and this solution was pipetted into 4500 mL of vigorously stirred heptane to precipitate the fluffy white product. After most of the heptane was decanted, the white precipitate was collected by filtration through a medium sintered glass funnel and subsequently dried under vacuum to give a white solid. The solid was purified by prep-HPLC (Phenomenex Gemini C18, 250x50mm, 10 mm column, 0.05% ammonium hydroxide in water / CH_3CN) and freeze-dried to afford 3.82 g of target compound as a yellow solid. ^{31}P NMR (162 MHz, CD_3CN) δ 167.1, 162.2. ^{1}H NMR (400 MHz, CD_3CN) δ 9.36 (br s, 1H), 8.63 (d, *J* = 16.51 Hz, 1H), 7.78-8.00 (m, 3H), 7.66 (t, *J* = 7.62 Hz, 1H), 7.42-7.57 (m, 4H), 7.24-7.40 (m,

7H), 6.89 (d, *J* = 8.68 Hz, 4H), 5.92-5.98 (m, 1H), 4.72-4.97 (m, 2H), 3.86-4.05 (m, 2H), 3.78 (2s, 6H), 3.27-3.70 (m, 3H), 2.87-3.20 (m, 12H), 2.67-2.82 (m, 2H), 1.54-1.79 (m, 4H).

SUPPLEMENTARY FIGURES

A

ID	Design[a]	IC_{50} (µM)	Tm[b] (°C)
Reference	G•C•a•a•g•c•a•t•c•c•t•G•T	2.9	56.2
ASO-1	G•C•a•a•g•c•a•t•c•c•t•G^{o}T	3.3	56.1
ASO-2	G^{o}C•a•a•g•c•a•t•c•c•t•G•T	1.7	57.6
ASO-3	G^{o}C•a•a•g•c•a•t•c•c•t•G^{o}T	2.1	56.7
ASO-4	G^{o}C^{o}a•a•g•c•a•t•c•c•t•G^{o}T	2.3	56.3

B

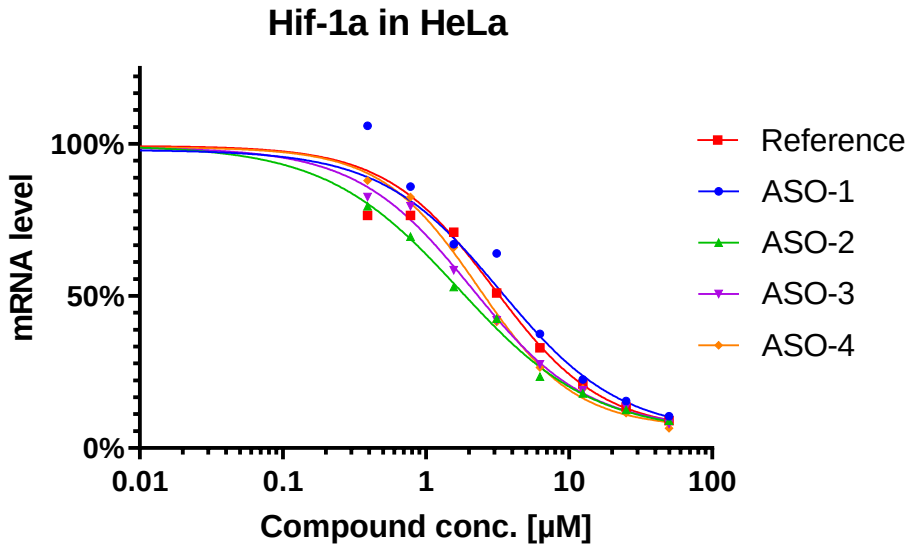

Figure S1. *In vitro Hif-1α* mRNA target reduction in HeLa cells after 72h of gapmer ASOs exposure under gymnotic uptake. **(A)** Design, antisense activity and Tm. Positions of phosphorodithioate (PS_2, ^{o}) are shown while the rest of ASO is stereorandom PS modified. [a] Upper case = LNA nucleotide; lower case = DNA nucleotide; stereorandom PS (•); phosphorodithioate (^{o}); [b] Melting temperature to complementary RNA (Tm); Complementary RNA strand for Tm measurement: ACAGGAUGCUUGC. **(B)** Dose-response curves for reducing *Hif-1α* mRNA in HeLa cells.

A

ID	Design[a]	IC_{50} (µM)	Tm[b] (°C)
Reference	G•A•G•t•t•a•c•t•t•g•c•c•a•A•C•T	0.27	62.9
ASO-1	G•A•G•t•t•a•c•t•t•g•c•c•a•A•C^{o}T	0.27	62.9
ASO-2	G^{o}A•G•t•t•a•c•t•t•g•c•c•a•A•C•T	0.24	62.9
ASO-3	G^{o}A•G•t•t•a•c•t•t•g•c•c•a•A•C^{o}T	0.33	63.0
ASO-4	G^{o}A•G•t•t•a•c•t•t•g•c•c•a•A^{o}C^{o}T	0.34	61.9
ASO-5	G^{o}A^{o}G•t•t•a•c•t•t•g•c•c•a•A•C^{o}T	0.36	61.5
ASO-6	G^{o}A^{o}G•t•t•a•c•t•t•g•c•c•a•A^{o}C^{o}T	0.42	61.2
ASO-7	G^{o}A^{o}G^{o}t•t•a•c•t•t•g•c•c•a•A^{o}C^{o}T	0.46	60.5

B

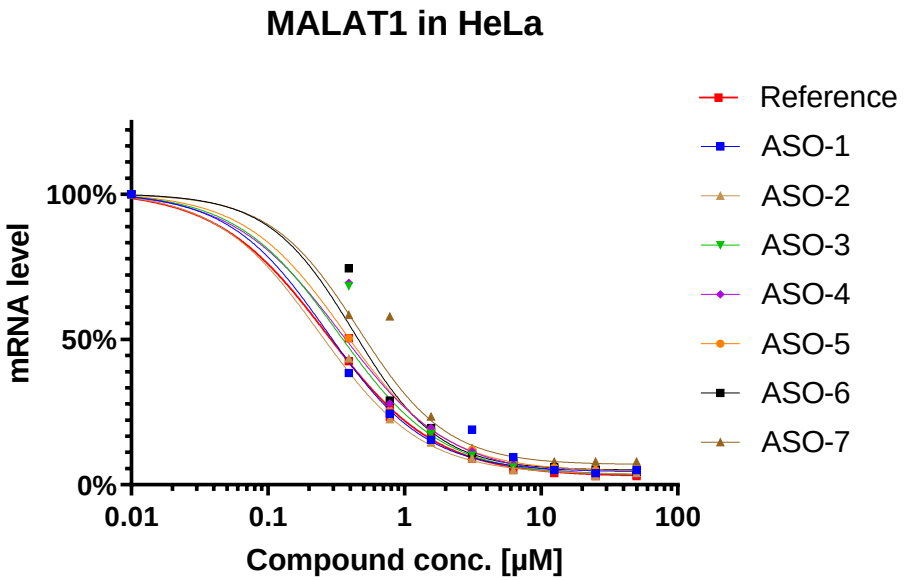

Figure S2. *In vitro Malat1* lncRNA target reduction in HeLa cells after 72h of gapmer ASOs exposure under gymnotic uptake. **(A)** Design, antisense activity and Tm. Positions of phosphorodithioate (PS_2, ^{o}) are shown while the rest of ASO is stereorandom PS modified. [a] Upper case = LNA nucleotide; lower case = DNA nucleotide; stereorandom PS (•); phosphorodithioate (^{o}); [b] Melting temperature to complementary RNA (Tm); Complementary

RNA strand for Tm measurement: AGUUGGCAAGUAACUC. **(B)** Dose-response curves for reducing *Malat1* lncRNA in HeLa cells.

A

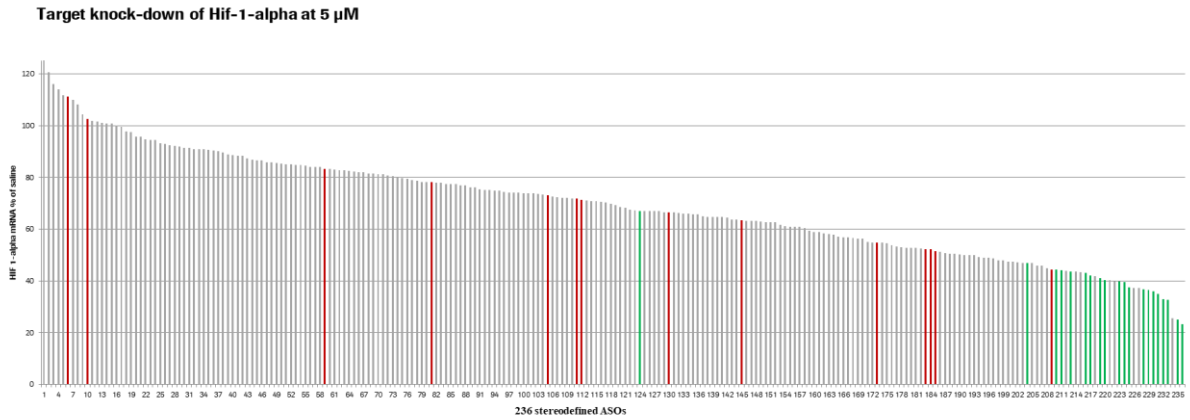

B

ID	Stereochemistry[a]	KD[b] (5 µM) %mRNA	ID	Stereochemistry[a]	KD[b] (5 µM) %mRNA
ASO-1	RSRR**RSSR**SRSS	23	ASO-18	SSSS**RSSR**RSSS	67
ASO-2	RSRR**RSSR**RSRS	25	ASO-19	RSRRR**RSSR**RSS	46
ASO-3	SRRS**RSSR**RRSS	33	ASO-20	RSRRR**RSSR**RSS	52
ASO-4	RSSR**RSSR**SSRR	33	ASO-21	RSRRR**RSSR**RSS	52
ASO-5	RRSR**RSSR**SSSS	35	ASO-22	RSRRR**RSSR**RSS	55
ASO-6	SSRS**RSSR**SRRS	36	ASO-23	RSRRR**RSSR**RSS	64
ASO-7	SRRR**RSSR**SRRR	36	ASO-24	RSRRR**RSSR**RSS	67
ASO-8	SRSS**RSSR**SRSS	37	ASO-25	RSRRR**RSSR**RSS	71
ASO-9	RRRS**RSSR**SRRS	38	ASO-26	RSRRR**RSSR**RSS	71
ASO-10	SSRS**RSSR**RSRR	40	ASO-27	RSRRR**RSSR**RSS	73
ASO-11	SRRS**RSSR**RSRS	40	ASO-28	RSRRR**RSSR**RSS	78
ASO-12	RRRS**RSSR**SRSR	42	ASO-29	RRRSS**RSSR**SSS	83
ASO-13	SSRS**RSSR**RSSS	43	ASO-30	SRRRR**RSSR**SSS	103
ASO-14	RRSS**RSSR**RRRS	44	ASO-31	RRRRS**RSSR**SSR	111
ASO-15	SSSS**RSSR**SSSR	44			
ASO-16	SRRS**RSSR**RSSS	45			
ASO-17	SRRS**RSSR**RSSR	47			

C

ID	Stereochemistry[a]	KD[b] (5 μM) %mRNA	ID	Stereochemistry[a]	KD[b] (5 μM) %mRNA
ASO-32	SSSSRRSSSSSR	129	ASO-57	SSSRSRSSSRRR	44
ASO-33	SRRSRSRSSRSS	121	ASO-58	SSRRSRSSSSRS	44
ASO-34	RSSRRRRRSSRR	116	ASO-59	SRRSRSRRSRSS	44
ASO-35	RRSSRSRSRSRS	114	ASO-60	SRSRRSSSRRRS	43
ASO-36	SRRRSSRRSRRR	112	ASO-61	RSSSRRSRSRSS	42
ASO-37	RRRRSRSSRSSR	111	ASO-62	RRSSRSRRRRSR	40
ASO-38	SSSRSSSRRRSR	110	ASO-63	RSRSRSRRRRSS	40
ASO-39	RRRSRSRSRSSR	108	ASO-64	RRSSRRSRSRRS	37
ASO-40	RRRSSSRRSSSS	104	ASO-65	RSRRRRRRRRSS	37
ASO-41	SRRRRRSSRSSS	103	ASO-66	RSSRRSRRSRSS	26
ASO-42	RSSSSSSSSSRS	102			
ASO-43	SSSRRRRSRRRR	102			
ASO-44	RRRRRRSRSSRR	101			
ASO-45	RRSRRSRSSRRR	101			
ASO-46	SRSRSRRSRSSS	101			
ASO-47	SRRRRRRSSRSR	100			
ASO-48	SSRSSSRSRSRS	100			
ASO-49	SRSSRRRSRRSR	98			
ASO-50	SSRRRRSSSSSR	98			
ASO-51	RRSSRRRSRSSS	96			
ASO-52	SSRRSRRSSRRS	96			
ASO-53	RRRSRRRRSSRS	95			
ASO-54	RSRRRSRSRRRS	94			
ASO-55	SSRSRSRRSSRR	94			
ASO-56	SSRRRRRRSRRR	93			

Figure S3. *In vitro Hif-1α* mRNA target reduction at 5 µM in HeLa cells after 72h of exposure (gymnotic uptake) with 236 ASOs differing only for their stereochemistry (conserved heterocyclic base sequence and DNA/LNA pattern). **(A)** Target knockdown of 236 fully stereodefined analogues targeting *Hif-1α* at 5 µM in HeLa cells. 236 fully stereodefined analogues were generated (5.7% of all possible LNAs isomers). PS stereochemistry in each position is randomly selected. From the data, broad potency range was observed for all 236 fully stereodefined analogues. **(B)** Stereochemistry designs and antisense activity in HeLa cells. It was observed that RSSR stereomotif in a specific position enhances chance of finding more potent ASOs. Green color bars identify ASOs where the RSSR stereochemical motif starts at position 5 in the stereochemical description (counting left to right - $R^1S^2R^3R^4$**R^5SSR**SRSS). Red color bars identify ASOs with the RSSR stereochemical motif starting at position 6 (counting left to right – $R^1S^2R^3R^4R^5$**R^6SSR**RSS). The target knock down histogram shows that ASOs with the stereochemical motif RSSR incorporated at position 5 (green label) elicit a more potent target reduction compared ASOs where the RSSR motif starts at position 6 (red label). [a] R-configuration (R); S-configuration (S); [b] Knockdown (KD, the remaining mRNA). (**C**) Selected stereodefined ASOs with poor knockdown (ASOs 32-56) and the ones with good knockdown (ASOs 57-66) don't contain RSSR motif at a specific position can greatly impact the potency. [a] R-configuration (R); S-configuration (S); [b] Knockdown (KD, the remaining mRNA).

A

ID	Design[a]	IC_{50} (µM)
Reference	G•C•a•a•g•c•a•t•c•c•t•G•T	3.18
ASO-1	G°C•a•a•g•c•a•t∧cVcVt∧G°T	3.59
ASO-2	G°C•a•a•g•c•a∧tVcVc∧t•G°T	2.66
ASO-3	G°C•a•a•g•c∧aVtVc∧c•t•G°T	2.02
ASO-4	G°C•a•a•g∧cVaVt∧c•c•t•G°T	1.03
ASO-5	G°C•a•a∧gVcVa∧t•c•c•t•G°T	4.18
ASO-6	G°C•a∧aVgVc∧a•t•c•c•t•G°T	4.36

B

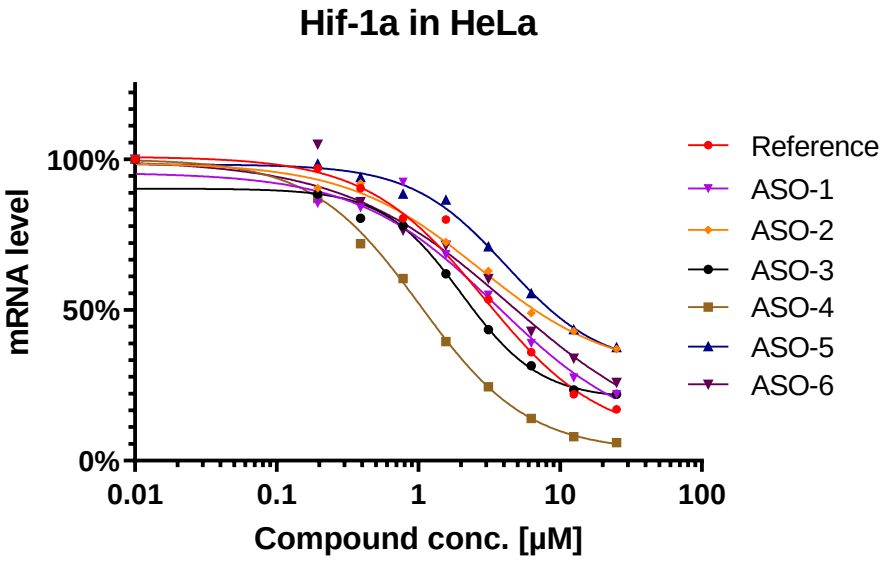

Figure S4. *In vitro Hif-1α* mRNA target reduction in HeLa after 72h of gapmer ASOs exposure under gymnotic uptake. **(A)** Design and antisense activity. Positions of phosphorodithioate (PS_2, °) and RSSR motif (∧ ∨ ∨ ∧**)** are shown while the rest of ASO is stereorandom PS modified. upper case = LNA nucleotide; lower case = DNA nucleotide; R-configuration (∧); S-configuration (∨); Phosphorodithioate linkage (°); Phosphorothioate linkage (•). **(B)** Dose-response curves for reducing *Hif-1α* mRNA in HeLa cells.

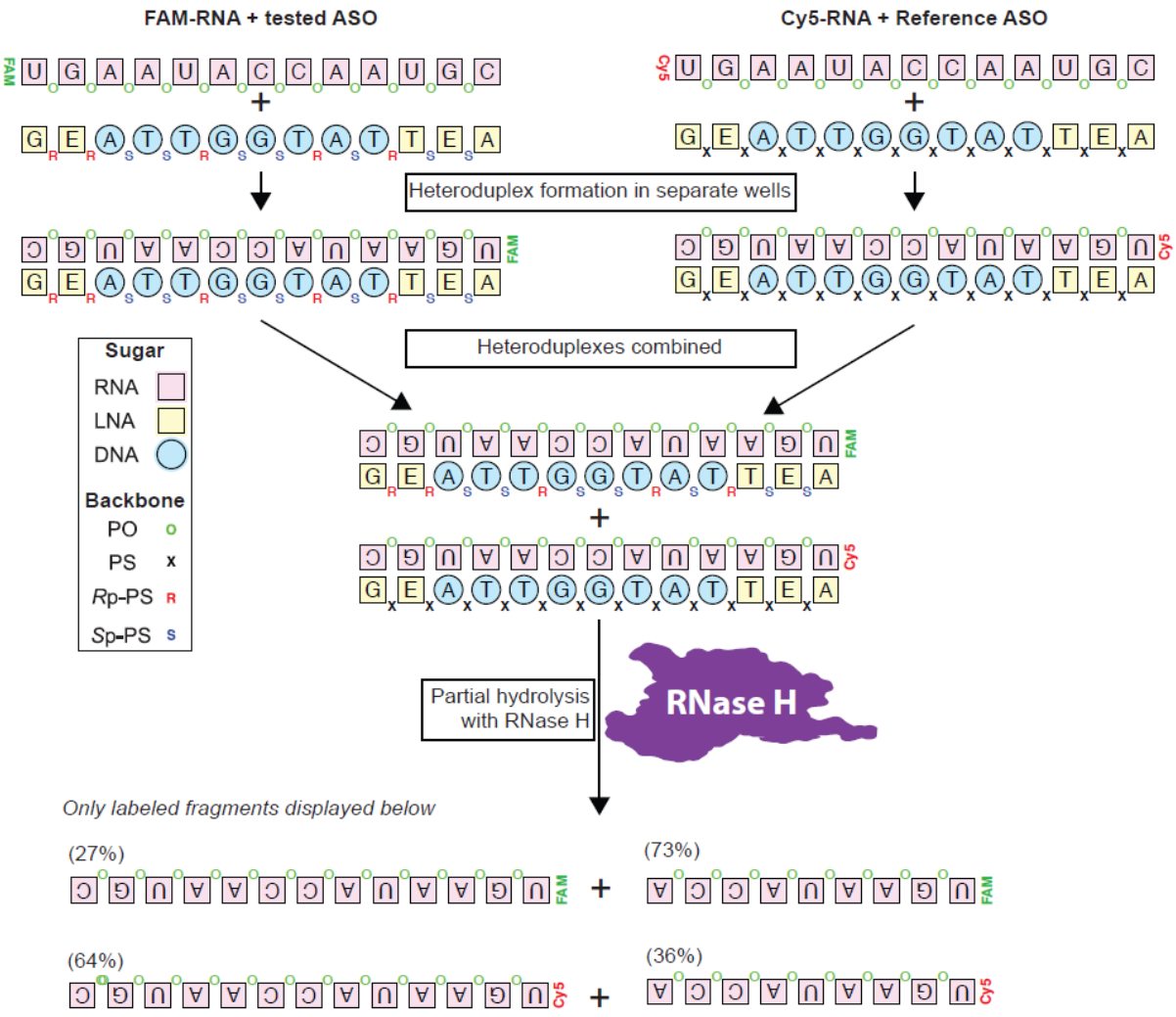

Figure S5 Demonstration of RNase H cleavage competition assay. For the heteroduplex formation, the reference ASO RTR3833 is annealed with Cy5-labeled complementary RNA strand, and the tested ASO is annealed with FAM-labeled complementary RNA strand. The equal amounts of these two heteroduplexes are mixed together, and treated with recombinant human RNase H1 solution. Reactions were terminated by addition of the stop solution. Samples were heat denatured and resolved on 15% polyacrylamide Urea-TBE gel. Gels were visualized for FAM and Cy5 channels using iBright™ FL1000 Imaging System (Thermo Fisher) and bands for full length and cleaved fractions were quantified using ImageJ.